

Negative kaons in dense baryonic matter

Evgeni E. Kolomeitsev*

*The Niels Bohr Institute, Blegdamsvej 17, DK-2100 Copenhagen, Denmark
and ECT*, Villa Tambosi, I-38050 Villazzano (TN), INFN G.C. Trento, Italy*

Dmitri N. Voskresensky

*Moscow Engineering Physical Institute, Kashirskoe shosse 31, RU-115409 Moscow, Russia
and GSI, Planck Str. 1, D-64291 Darmstadt, Germany*

(Received 26 November 2002; published 29 July 2003)

The kaon polarization operator in dense baryonic matter of arbitrary isotopic composition is calculated including s - and p -wave kaon-baryon interactions. The regular part of the polarization operator is extracted from the realistic kaon-nucleon interaction based on the chiral and $1/N_c$ expansion. Contributions of $\Lambda(1116)$, $\Sigma(1195)$, $\Sigma^*(1385)$ resonances are taken explicitly into account in the pole and regular terms with the inclusion of mean-field potentials. The baryon-baryon correlations are incorporated and fluctuation contributions are estimated. Results are applied for K^- in neutron star matter. Within our model a second-order phase transition to the s -wave K^- condensate state occurs at $\rho_c \gtrsim 4\rho_0$ with baryon-baryon correlations included. We show that a second-order phase transition to the p -wave K^- condensate state may occur at densities $\rho_c \sim (3-5)\rho_0$ dependent on the parameter choice. We demonstrate that a first-order phase transition to a proton-enriched (approximately isospin-symmetric) nucleon matter with a p -wave K^- condensate can occur at smaller densities, $\rho \lesssim 2\rho_0$. The transition is accompanied by the suppression of hyperon concentrations.

DOI: 10.1103/PhysRevC.68.015803

PACS number(s): 26.60.+c, 13.75.Jz, 21.65.+f, 97.60.Jd

I. INTRODUCTION

Strangeness modes in compressed hadronic matter have been the focus of interests during the last decade. Strangeness is considered to be a good probe of the dynamics of heavy-ion collisions. A vast amount of data is already accumulated for different collision energy regimes at GANIL, GSI, CERN, and BNL facilities [1], and new data are in advent [2]. Understanding strangeness production requires a systematic study of the evolution of virtual strangeness modes in the quark-gluon plasma and in the soup of virtual hadrons. At the breakup stage, these virtual modes are redistributed between real strange particles which can be observed in experiment.

Another interesting topic is the strangeness content of neutron stars. With an increasing density, strangeness shows up in the filling of the hyperon Fermi seas and/or in the creation of a kaon condensate. A better understanding of the topics mentioned above needs more in-depth knowledge of the kaon-baryon interaction in dense baryonic matter. The possibility of kaon condensation in dense nuclear matter was risen in Refs. [3,4]. Kaon condensation in neutron star interiors may have interesting observational consequences: (i) The softening of the equation of state (EoS) due to the appearance of a kaon condensate phase lowers the maximum neutron star mass and can induce the transformation of neutron stars into low-mass black holes [5]; (ii) Kaon condensation is predicted to be accompanied with the change of the nucleon isospin composition from a neutron-enriched star ($N \gg Z$) to a “nuclear” star ($N \sim Z$) or even to a “proton”

star ($N \lesssim Z$), where the electric charge of protons is compensated by the charge of the condensed kaons [6]; (iii) The enhanced neutrino-emission processes occurring on protons in proton-enriched matter and on the kaon condensate field lead to substantially faster cooling of the star [7].

The K^- condensate is created in neutron stars through weak multiparticle processes

$$e^- + X \rightarrow K^- + X', \quad n + X \rightarrow p + K^- + X', \quad (1)$$

in which electrons are replaced by K^- mesons and neutrons are converted into protons and K^- [8]. The symbolic writing (1) assumes that surrounding baryons (X, X') assure the momentum conservation, and thus, the critical point is determined by the energy balance only. These processes become possible if the electron chemical potential μ_e exceeds the minimal K^- energy,

$$\omega^{\min}(\vec{k}_m) = \min_{\vec{k}} \{ \omega^{\min}(\vec{k}) \},$$

where $\omega^{\min}(\vec{k})$ is the K^- energy at the lowest quasiparticle branch of the spectrum of K^- excitations in neutron star matter. In Refs. [4,8,9] it has been postulated that there is only one kaon branch, for which $\omega(\vec{k}=0) \rightarrow m_K$ (m_K is the kaon mass) as the baryon density $\rho \rightarrow 0$, and the minimum is achieved at $\vec{k}_m = 0$. The critical point of the s -wave K^- condensation in a second-order phase transition is determined by the condition $\omega(\vec{k}=0) = \mu_e$. A first-order phase transition to the kaon condensate state was investigated in Ref. [10] applying the Maxwell construction principle and in Ref. [11]

*Email address: E.Kolomeitsev@nbi.dk

according to the Gibbs criteria. The p -wave kaon-nucleon interaction, which changes the kaon spectrum at finite momenta was disregarded in those works. The p -wave $\Lambda(1116)$ -nucleon-hole and $\Sigma(1195)$ -nucleon hole contributions to the kaon polarization operator were introduced in Ref. [12] in the framework of the chiral SU(3) symmetry. However, the authors of Ref. [12] focused on the discussion of the s -wave kaon condensation only, and considered the polarization operator at zero momentum.

In Ref. [6], we worked out a possibility for the p -wave kaon condensation. The kaon polarization operator was constructed with the inclusion of the $\Lambda(1116)$ -nucleon-hole and $\Sigma(1195)$ -nucleon-hole contributions in the p -wave part of the kaon polarization operator and the kaon-pion and kaon-kaon interactions. The multibranch spectrum of K^- mesons was found and the possibility of the p -wave kaon condensation related to the population of hyperon-nucleon-hole modes was demonstrated. Possibilities of the first-order phase transitions in neutron star interiors to a proton-enriched matter with a p -wave K^- condensate and to a neutron-enriched matter with a p -wave \bar{K}^0 condensate were investigated.

The case of a large hyperon admixture in the neutron star core was considered in Ref. [13]. In such a medium both the K^- and the K^+ spectra possess extra branches associated with the particle-hole excitations $\Xi - \Lambda^{-1}$, $\Xi - \Sigma^{-1}$ for K^- and $N - \Lambda^{-1}$, $N - \Sigma^{-1}$ for K^+ [hole states are labeled here by (-1)]. At large kaon momenta, the branches of K^+ and K^- spectra merge, signaling an instability with respect to K^+K^- pair creation.

The analysis in Refs. [6,13] relied heavily on the pole approximation for the particle-hole diagrams. Final width effects were thereby disregarded too. The presence or absence of quasiparticle branches in the K^- spectrum depends on the kaon energy and on the strength of the s - and p -wave attraction [14]. The short-range baryon-baryon correlations, which, as a rule, suppress the attraction, were not included in Refs. [6,13]. The role of the correlations for the p wave has been investigated in Ref. [15]. However, the relative strength of the s - and p -wave attraction remained model dependent because no systematic investigation of the kaon-nucleon interaction including s and p waves was available at that time.

Recently, the kaon-nucleon scattering has been studied in the framework of a relativistic chiral SU(3) Lagrangian imposing constraints from the K^+ -nucleon and pion-nucleon sectors [16]. The covariant coupled-channel Bethe-Salpeter equation was solved with the interaction kernel truncated to the third chiral order including the terms which are leading in the large N_c limit of QCD. All SU(3) symmetry-breaking effects are well under control by the combined chiral and large N_c expansions. This analysis gives an opportunity to extend the results of Refs. [6,15] taking into account off-pole (regular background) contributions to the kaon self-energy. The accurate fit to experimental data achieved in Ref. [16] fixes the values of the kaon-nucleon-hyperon coupling constants. Particularly, the $\Sigma^*(1385)$ -pole contribution to the kaon-nucleon scattering was proved to be sizable, and was not included in Refs. [6,13].

The discussion of the s -wave and, especially, of the p -wave kaon-baryon interactions in nuclear matter is important for the kaon production in heavy-ion collisions [17]. The momentum dependence of kaon yields is experimentally measured [18]. Also, the multibranch K^- spectrum can be tested via $\bar{\nu}$ scattering on atomic nuclei [15]. Peculiarities of the K^- -nucleon interaction near the mass shell are of great importance for the physics of K^- atoms [19,20].

This paper is structured as follows. In Sec. II, we describe baryon matter within a relativistic mean-field model. In Sec. III, we introduce the kaon-nucleon interaction in vacuum following the partial-wave analysis of Ref. [16]. Then, we separate the pole contributions of $\Lambda(1116)$, $\Sigma(1195)$, and $\Sigma^*(1385)$ hyperons in p waves. Sections IV through VII are devoted to the construction of the kaon polarization operator. In Sec. IV, we build the polarization operator in the gas approximation, but including the mean-field potentials that act on baryons. Besides the $\Lambda(1116)$, $\Sigma(1195)$, and $\Sigma^*(1385)$ -nucleon-hole contributions the polarization operator contains a regular attractive part that is weakly dependent on the kaon energy. In Sec. V, we separate the s - and p -wave parts of the kaon polarization operator. The occupation of hyperon Fermi seas is incorporated in Sec. VI. Repulsive baryon-baryon correlations are evaluated and included in the hyperon-nucleon particle-hole channels and in the regular part of the polarization operator in Sec. VII. In each of these sections, we illustrate the strength of new terms included into the polarization operator and suggest effective parametrizations. We relegate the discussion of contributions from kaon fluctuations (baryon self-energies, multiloop corrections) to Appendix C. We argue that these effects do not modify substantially the kaon polarization operator at zero temperature in the region of small kaon energies and momenta, which is of our interest here. In Sec. VIII, we analyze different possibilities for the second- and first-order phase transitions to the s - and p -wave K^- condensates. Particularly, we argue for the p -wave K^- condensation at $\rho \lesssim 2\rho_0$ ($\rho_0 \approx 0.17 \text{ fm}^{-3}$ is the density of nuclear saturation) arising via a first-order phase transition. In this phase transition, all the hyperon Fermi seas are melted and neutron star matter becomes proton enriched with an approximately symmetric-isospin composition, $N \approx Z$. In Appendix A, we discuss how the results depend on the specifics of the EoS. Some technical information on the Green's functions is provided in Appendix B. Throughout this paper, we use units of $\hbar = c = 1$.

Although a number of new effects are incorporated in our scheme some other effects not included here might be also important. The present calculations suffer from many uncertainties, most of which are due to the lack of experimental information on the coupling constants, the absence of unambiguous way for going off-mass shell and the lack of study of more complicated in-medium fluctuation effects, which we just roughly estimated in the present work. Among them, there are the pion softening effects [21], which can significantly affect the results at finite temperatures, and the contribution of nonlinear meson-meson interactions. The latter may partially suppress the condensate contribution to the energy at densities above the critical one.

II. BARYON INTERACTION IN RELATIVISTIC MEAN-FIELD MODEL

A. Lagrangian of the model

We consider a dense system consisting of baryons and leptons, which we describe by a Lagrangian density containing a baryon and a lepton contribution $\mathcal{L} = \mathcal{L}_B + \mathcal{L}_l$.

It is convenient to describe the baryon matter at densities relevant for neutron star interiors by the mean-field solution of the Lagrangian [22],

$$\begin{aligned} \mathcal{L}_B = & \sum_B \bar{B}(i\partial - g_{\omega B}\omega - g_{\rho B}\vec{\rho} \cdot \vec{t}_B - m_B + g_{\sigma B}\sigma)B \\ & + \frac{\partial_\mu \sigma \partial^\mu \sigma}{2} - \frac{m_\sigma^2 \sigma^2}{2} - \frac{m_N b (g_{\sigma N} \sigma)^3}{3} - \frac{c (g_{\sigma N} \sigma)^4}{4} \\ & - \frac{\omega_{\mu\nu} \omega^{\mu\nu}}{4} + \frac{m_\omega^2 \omega_\mu \omega^\mu}{2} - \frac{\vec{\rho}_{\mu\nu} \vec{\rho}^{\mu\nu}}{4} + \frac{m_\rho^2 \vec{\rho}_\mu \vec{\rho}^\mu}{2}, \end{aligned} \quad (2)$$

where all states of the baryon ($J^P = \frac{1}{2}^+$) octet $B = (n, p, \Lambda, \Sigma^{\pm, 0}, \Xi^{-0})$ interact via exchanges of scalar, vector, and isovector mesons σ , ω_μ , $\vec{\rho}_\mu$. Heavier baryons do not appear at baryon densities under consideration ($\rho \leq 6\rho_0$) and, therefore, are not included. In Eq. (2), \vec{t}_B denotes the isospin operator acting on the baryon B . The field-strength tensors for the vector mesons are given by $\omega_{\mu\nu} = \partial_\mu \omega_\nu - \partial_\nu \omega_\mu$ for the ω mesons and $\vec{\rho}_{\mu\nu} = \partial_\mu \vec{\rho}_\nu - \partial_\nu \vec{\rho}_\mu$ for the ρ mesons. Equations of motion for the baryons follow from Eq. (2), and give

$$E_B(\vec{p}) = \epsilon_B(\vec{p}) + V_B, \quad \epsilon_B(\vec{p}) = \sqrt{m_B^{*2} + \vec{p}^2}, \quad (3)$$

where $m_B^* = (m_B - g_{\sigma B}\sigma)$ is the baryon effective mass and $V_B = g_{\omega B}\omega_0 + g_{\rho B}\rho_{03}t_{3B}$, with $\sigma, \omega_0, \rho_{03}$ being the mean-field solutions of the equations of motion for the meson fields. The composition of the cold neutron star matter at baryon density ρ is determined by the β -equilibrium conditions $E_B(p_{FB}) = \mu_n - q_B \mu_e$. Here, p_{FB} is the Fermi momentum, q_B is the electric charge of a given baryon species B , and μ_n, μ_e are the chemical potentials of neutrons and electrons determined by the total baryon density ρ and the electroneutrality condition.

The lepton Lagrangian density is the sum of the electron and the μ^- meson contributions $\mathcal{L}_l = \mathcal{L}_e + \mathcal{L}_\mu$. In β equilibrium $\mu_\mu = \mu_e$, and muons appear in the system only when μ_e exceeds the muon mass m_μ .

The energy density of the system is given by

$$E_{\text{tot}} = E_{\text{mes}} + \sum_B E_B^{\text{kin}}(p_{FB}) + \sum_{l=e^-, \mu^-} E_l(\mu_e),$$

$$\begin{aligned} E_{\text{mes}} = & \frac{1}{3} b m_N (g_{\sigma N} \sigma)^3 + \frac{1}{4} c (g_{\sigma N} \sigma)^4 + \frac{1}{2} m_\sigma^2 \sigma^2 + \frac{1}{2} m_\omega^2 \omega_0^2 \\ & + \frac{1}{2} m_\rho^2 \rho_{03}^2, \end{aligned}$$

$$E_B^{\text{kin}}(p_{FB}) = \frac{1}{\pi^2} \int_0^{p_{FB}} dp p^2 \epsilon_B(p),$$

$$E_l(\mu_l) = \frac{1}{\pi^2} \theta(\mu_l - m_l) \int_{m_l}^{\mu_l} d\epsilon \epsilon^2 \sqrt{\epsilon^2 - m_l^2}, \quad (4)$$

where $\theta(x)$ is the step function.

B. Coupling constants

The coupling constants in Eq. (2) are adjusted such as to reproduce properties of the equilibrium nuclear matter: saturation density ρ_0 , binding energy E_{bind} , compressibility modulus K , and effective nucleon mass $m_N^*(\rho_0)$. In the following, we use the values $\rho_0 = 0.17 \text{ fm}^{-3}$ and $E_{\text{bind}} = -16 \text{ MeV}$. For the nuclear compressibility modulus, we take the value $K = 210 \text{ MeV}$, which follows from the variational calculation [23]. Following Ref. [22], we adopt the symmetry energy $a_{\text{sym}} = 36.8 \text{ MeV}$ which lies within the interval allowed by microscopic calculations [24]. We take the effective nucleon mass $m_N^*(\rho_0) = 0.85 m_N$, cf. argumentation in Ref. [21]. For discussion of uncertainties in the choices of parameters, we refer the interested reader to Ref. [25].

The corresponding coupling constants of Lagrangian (2) are

$$\begin{aligned} \frac{g_{\omega N}^2 m_N^2}{m_\omega^2} = 54.60, \quad \frac{g_{\sigma N}^2 m_N^2}{m_\sigma^2} = 164.5, \quad \frac{g_{\rho N}^2 m_N^2}{m_\rho^2} = 121.7, \\ b = 0.02028, \quad c = 0.04716. \end{aligned} \quad (5)$$

In order to verify the sensitivity of the results to details of the EoS, we explore another set of the parameters in Appendix A, which is fitted to reproduce the microscopic calculations of the Urbana-Argonne group [26].

When including hyperons, one also has to specify the hyperon couplings to the meson fields, $x_{MH} = g_{MH}/g_{MN}$ with $M = (\sigma, \omega, \rho)$ and $H = (\Lambda, \Sigma, \Xi)$. Couplings to the vector mesons are estimated from the quark counting as $x_{\omega\Lambda(\Sigma)} = x_{\rho\Sigma} = \frac{2}{3}$ and $x_{\omega\Xi} = x_{\rho\Xi} = \frac{1}{3}$. Alternatively, relying on the SU(3) symmetry [27], one would find $x_{\rho\Sigma} = x_{\rho\Xi} = 1$ for the ρ meson couplings. The scalar meson couplings can be constrained by making use of hyperon binding energies in infinite nuclear matter at saturation [28], extrapolated from hypernucleus data. For the given hyperon binding energy E_{bind}^H , we have the following relation between the scalar and vector couplings:

$$\begin{aligned} E_{\text{bind}}^H = & (g_{\omega N}^2 \rho_0 / m_\omega^2) x_{\omega H} - (m_N - m_N^*) x_{\sigma H} \\ = & (80.73 x_{\omega H} - 140.70 x_{\sigma H}) \text{ MeV}. \end{aligned}$$

There is convincing evidence from the systematic study of hypernuclei that for Λ particles $E_{\text{bind}}^\Lambda \simeq -30 \text{ MeV}$ [29]. For Σ hyperons in nuclei, on the other hand, the data are still controversial, giving the broadband, $-10 \text{ MeV} < E_{\text{bind}}^\Sigma < 30 \text{ MeV}$, from a slight attraction to a strong repulsion [30]. Following Ref. [31], we adopt for Ξ the value $E_{\text{bind}}^\Xi \simeq -18 \text{ MeV}$ advocated also in Ref. [27].

To cover different possibilities we consider four cases.

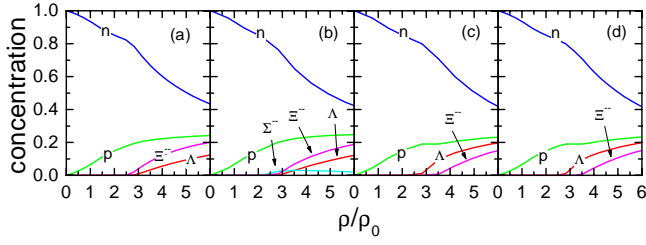


FIG. 1. Concentration of baryon species in neutron star matter. Four panels correspond to the four choices of the hyperon-nucleon interaction constants (cases I–IV) specified in text.

Case I: vector meson couplings are taken according to the quark counting, $x_{\omega\Lambda(\Sigma)} = x_{\rho\Sigma} = 2x_{\omega\Sigma} = 2x_{\rho\Sigma} = \frac{2}{3}$ and $E_{\text{bind}}^{\Lambda} = -30$ MeV, $E_{\text{bind}}^{\Xi} = -18$ MeV, $E_{\text{bind}}^{\Sigma} = 30$ MeV.

Case II: the same as in case I but $E_{\text{bind}}^{\Sigma} = -10$ MeV.

Case III: the same as in case I but the ρ meson couplings are taken according to the SU(3) symmetry, i.e., $x_{\rho\Sigma, \Xi} = 1$.

Case IV: the same as in case III, but for $E_{\text{bind}}^{\Sigma} = -10$ MeV.

C. Particle concentrations

In Fig. 1, we show the resulting concentrations of different baryon species as function of the baryon density. Panels (a)–(d) correspond to the four choices of the hyperon-meson coupling constants specified above. We see that hyperons appear in neutron star matter in all cases at density $\rho > \rho_{c,H} \approx (2.5-3)\rho_0$. The latter value is rather insensitive to various choices of hyperon-nucleon interactions. However, the order in which hyperons populate the Fermi seas depends crucially on the details of hyperon-nucleon interactions. The Σ^- hyperons do not appear at least up to $6\rho_0$, except for case II. However, even in case II their concentration is very small. The place of Σ^- is readily taken by Ξ^- and Λ hyperons. This observation is in line with the results of Ref. [32]. In case IV, we choose $E_{\text{bind}}^{\Sigma} < 0$, but Σ hyperons do not appear due to the increasing repulsion mediated by ρ mesons with larger coupling constants than in case II. We see that in cases I–IV, the proton concentration saturates when hyperons appear in the system. We also see that none of the choices I–IV support effects observed in Ref. [13], where Λ hyperons become more abundant than protons already at $3\rho_0$. Therefore, the p -wave K^+K^- condensation discussed in Ref. [13] does not show up in the framework of our model for all four parameter choices.

III. K^- -NUCLEON INTERACTION IN VACUUM

The kaon-nucleon interaction in vacuum results as the solution of the coupled-channel Bethe-Salpeter equation

$$\begin{array}{c} M \\ \diagdown \\ \triangle \\ \diagup \\ M' \\ B \quad B' \end{array} = \begin{array}{c} M \\ \diagdown \\ \circ \\ \diagup \\ M' \\ B \quad B' \end{array} + \sum_{M'', B''} \begin{array}{c} M \\ \diagdown \\ \triangle \\ \diagup \\ M' \\ B \quad B'' \end{array} \quad .$$

(6)

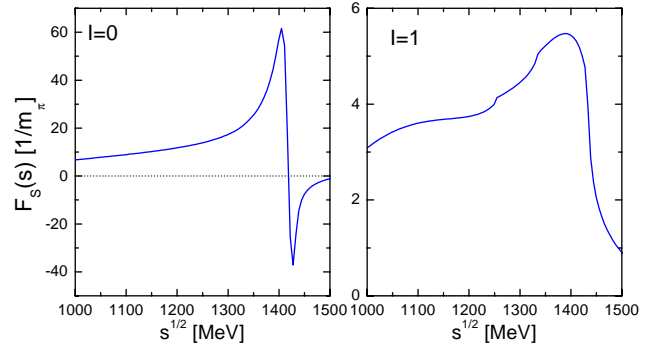


FIG. 2. Real parts of the s -wave KN scattering amplitudes in isospin-zero and isospin-one channels [16].

Here, the triangle is the full meson-baryon scattering amplitude with strangeness -1 and the circle stands for the interaction kernel. This equation involves rescatterings through all possible meson-baryon intermediate states allowed by the strangeness conservation. The interaction kernel can be derived from the SU(3) chiral Lagrangians [33–36] or can be phenomenologically adjusted to fit the data within the K -matrix formalism [37,38].

In view of the general interest to the s -wave kaon condensation prevailing in the literature so far, most of the attention has been paid to the kaon-nucleon interaction in the s wave. Although far below the threshold the s -wave kaon-nucleon scattering amplitude is a rather smooth function of the kaon energy, close to the threshold the amplitudes vary strongly due to the $\Lambda(1405)$ resonance (see Fig. 2). Therefore, the extrapolation into the subthreshold region of the scattering amplitude, adjusted to fit the data above the K^-N threshold, crucially depends on the microscopic model applied. Its in-medium modification is a matter of debate too [39–43].

Up to recently, only scarce information on the p -wave kaon-nucleon interaction was available. In the isospin-zero channel, the small p -wave amplitudes were not separated from the large contribution of the $\Lambda(1405)$ resonance in the s wave, which dominates near threshold energies. In the isospin-one channel, determination of the p -wave amplitudes remained also uncertain due to a lack of direct experimental information on the K^-n scattering at low energies. This gap was filled in Ref. [16], where the $\bar{K}N$ interaction was obtained as a solution of the covariant coupled-channel Bethe-Salpeter equation with a kernel derived from a relativistic chiral SU(3) Lagrangian with extra constraints from the K^+ nucleon and pion-nucleon sector. This analysis provides reliable estimates for both the s - and p -wave K^-N scattering amplitudes, which we will use in the following.

A. Forward scattering amplitudes

The vacuum $\bar{K}N$ forward scattering amplitudes in a given isospin channel I have the following contributions from s - and p -partial waves:

$$T^{(I)}(s) = T_S^{(I)}(s) + T_P^{(I)}(s) = \frac{\bar{E}(s, m_N^2, m_K^2) + m_N}{2m_N} \times [F_S^{(I)}(s) + Q^2(s, m_N^2, m_K^2)F_P^{(I)}(s)],$$

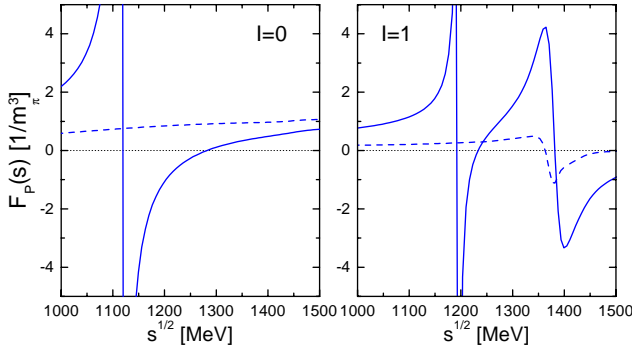


FIG. 3. Real parts of the p -wave KN scattering amplitudes F_p in isospin-zero and isospin-one channels (solid lines) [16]. The dashed lines represent the corresponding pole-subtracted scattering amplitudes (9).

$$Q^2(s, p^2, k^2) = \frac{(s - p^2 - k^2)^2 - 4k^2 p^2}{4s}, \quad (7)$$

where $s = (p + k)^2$, and $p = (\epsilon_N(\vec{p}), \vec{p})$, $k = (\omega, \vec{k})$ are the four-momenta of the incoming nucleon and kaon, respectively. For nucleons and kaons on mass shell, the quantity $Q^2(s, m_N^2, m_K^2)$ is the square of the center-of-mass momentum in the kaon-nucleon channel, $\bar{E}(s, m_N^2, m_K^2) = \sqrt{m_N^2 + Q^2(s, m_N^2, m_K^2)}$ is the nucleon energy in the center-of-mass frame, $\bar{E}(s, p^2, k^2) = (s + p^2 - k^2)/2\sqrt{s}$, m_N and m_K are the free nucleon and kaon masses. We shall neglect the isospin-symmetry breaking within kaon and nucleon isospin multiplets, which is irrelevant in dense nuclear matter.

The invariant partial-wave amplitudes $F_S^{(l)}$ and $F_P^{(l)}$ are related to the standard partial-wave amplitudes (see Ref. [44] Sec. 3.1 for definitions) as

$$F_S^{(l)}(s) = \frac{8\pi\sqrt{s}}{\bar{E}_+(s, m_N^2, m_K^2)} f_{0+}^{(l)}(s),$$

$$F_P^{(l)}(s) = \frac{8\pi\sqrt{s}Q^2(s, m_N^2, m_K^2)}{\bar{E}_+(s, m_N^2, m_K^2)} [f_{1-}^{(l)}(s) + 2f_{1+}^{(l)}(s)]. \quad (8)$$

The partial amplitudes $f_{l\pm} = f_{l, J=l\pm\frac{1}{2}}$ in Eq. (8) are the scattering amplitudes for given angular momentum l and total momentum J , and $\bar{E}_\pm(s, p^2, k^2) = \bar{E}(s, p^2, k^2) \pm \sqrt{p^2}$. The real parts of the partial amplitudes $T_S^{(l)}$ and $T_P^{(l)}$ are shown in Figs. 2 and 3 by solid lines. The pronounced peak structures in the p -wave amplitude are due to the $\Lambda(1116)$ pole in the isospin-zero channel, and the $\Sigma(1195)$ and $\Sigma^*(1385)$ poles in the isospin-one channel.

B. Separation of the pole terms

The hyperon s -channel exchanges are responsible for the strongest variation of the polarization operator at low frequencies and momenta. Therefore, they deserve a special consideration in view of the baryon modifications by the mean-field potentials. To treat them explicitly, we separate

the pole contributions from the p -wave amplitudes. We define the pole and pole-subtracted amplitudes

$$\delta F_P^{(l)}(s) = F_P^{(l)} - F_{\text{pole}}^{(l)}(s), \quad (9)$$

$$F_{\text{pole}}^{(0)}(s) = -2 \frac{C_{KN\Lambda}^2 2m_\Lambda}{\bar{E}_+^2(s, m_N^2, k^2)} \frac{(m_\Lambda + m_N)^2}{s - m_\Lambda^2 + i0}, \quad (10)$$

$$F_{\text{pole}}^{(1)}(s) = -4 \frac{C_{KN\Sigma}^2 m_\Sigma}{\bar{E}_+^2(s, m_N^2, m_K^2)} \frac{(m_\Sigma + m_N)^2}{s - m_\Sigma^2 + i0}$$

$$- \frac{8}{3} \frac{C_{KN\Sigma^*}^2 (s/m_{\Sigma^*})}{s - m_{\Sigma^*}^2 + \frac{i}{2} \gamma_{\Sigma^*}(s)} \frac{\bar{E}_+(m_{\Sigma^*}^2, m_N^2, m_K^2)}{\bar{E}_+(s, m_N^2, m_K^2)}. \quad (11)$$

The Σ^* width, $\gamma_{\Sigma^*}(s) = (\sqrt{s} + m_{\Sigma^*})[\gamma_{\pi\Lambda}(s) + \gamma_{\pi\Sigma}(s) + \gamma_{KN}(s)]$, includes contributions from $\pi\Lambda$, $\pi\Sigma$, and KN channels, $\gamma_{\phi B}(s) = C_{\phi B\Sigma^*}^2 \bar{E}_+(s, m_B^2, m_\phi^2) |Q(s, m_B^2, m_G^2)|^3 / (12\pi\sqrt{s})$, where m_B is the mass of the corresponding baryon $B = (n, p, \Lambda, \Sigma^{\pm, 0}, \Xi^{-0})$ and m_ϕ is the mass of the corresponding light meson $\phi = (\pi, K)$. The coupling constants $C_{\pi\Lambda(\Sigma)\Sigma^*}$ can be extracted from the partial width of the Σ^* hyperon. The values of the $KN\Lambda(\Sigma)$ coupling constants $C_{KN\Lambda} \approx -0.68/m_\pi$, $C_{KN\Sigma} \approx 0.34/m_\pi$ entering Eqs. (10) and (11) follow directly from the amplitudes shown in Fig. 3. The values of $C_{KN\Lambda}$ and $C_{KN\Sigma}$ are defined as couplings of Λ to $(K^\dagger N)$ and Σ^α to $(K^\dagger \tau^\alpha N)$ isospin states, where K, N stand for the isospin doublets, Σ^α is the isospin triplet, and τ^α are the isospin Pauli matrices. Note that the value of $C_{KN\Lambda}$, obtained on the basis of Ref. [16], is smaller than that fitted by the Jülich group [45] and used in Refs. [12,6].

The scattering amplitude near the Σ^* resonance can be only approximately described by the last term in Eq. (11), since the corresponding amplitude results from a multichannel dynamics, which generates the energy-dependent self-energy of the Σ^* resonance. This self-energy, however, can be neglected at \sqrt{s} relevant for the calculations below. Reference [16] gives for the Σ^* resonance coupling $C_{KN\Sigma^*} \approx 0.84/m_\pi$ defined by the Lagrangian term $C_{KN\Sigma^*} \bar{\Sigma}_\mu^{\alpha} \partial^\mu K^\dagger \tau^\alpha N$. The pole subtracted amplitudes $\delta F^{(l)}(s)$ are shown in Fig. 3 by dashed lines. We see that the amplitudes in both isospin channels are smooth functions of \sqrt{s} in the subthreshold region $\sqrt{s} < 1300$ MeV of our interest. Note that the procedure of pole subtraction is not unambiguous. Forms (10) and (11) are chosen here for a later convenience, since they allow direct comparison with the analysis of Refs. [6,14,13].

To consider the kaon-nucleon interaction in dense matter, we also need to take into account the mean-field potentials acting on baryons according to Lagrangian (2).

IV. K^- POLARIZATION OPERATOR FROM SCATTERING AMPLITUDES

A. Gas approximation and baryonic mean fields

Our next aim is to construct the retarded K^- polarization operator in baryonic matter, $\Pi_R^{\text{tot}}(\omega, \vec{k})$, related to the kaon propagator as $D_K^{-1}(\omega, \vec{k}) = \omega^2 - \vec{k}^2 - m_K^2 - \Pi_R^{\text{tot}}(\omega, \vec{k})$. The spectral function is determined as $A_K(\omega, \vec{k}) = -2\text{Im}D_K(\omega, \vec{k})$. Quasiparticle branches of the spectrum appear in the energy-momentum region where the kaon width $\Gamma_K = -2\text{Im}\Pi_R^{\text{tot}}(\omega, \vec{k})$ is much smaller than any other typical energy scale. Then, one can put $\Gamma_K \rightarrow 0$ in the kaon Green's function and the quasiparticle branches are given by the dispersion equation $\text{Re}D_K^{-1}(\omega, \vec{k}) = 0$.

From the vacuum scattering amplitudes, we can construct the causal polarization operator $\Pi_C^{(0)}(\omega, \vec{k})$ related to the partial-wave amplitudes, $F_S^{(1)}$ and $F_P^{(1)}$ in the gas approximation

$$\Pi_C^{(0)}(\omega, \vec{k}) = I_{\text{s wave}}(\omega, \vec{k}) + I_{\text{p wave}}(\omega, \vec{k}), \quad (12)$$

$$\begin{aligned} I_{\text{s wave}}(\omega, \vec{k}) &\equiv I_{\text{s wave}, p}(\omega, \vec{k}) + I_{\text{s wave}, n}(\omega, \vec{k}) \\ &= - \int \frac{2d^3\vec{p}}{(2\pi)^3} \frac{\bar{E}_+(s, m_N^2, k^2)}{2\sqrt{m_N^2 + \vec{p}^2}} \left\{ \frac{1}{2} [F_S^{(0)}(s) \right. \\ &\quad \left. + F_S^{(1)}(s)] n_p(\vec{p}) + F_S^{(1)}(s) n_n(\vec{p}) \right\}, \quad (13) \end{aligned}$$

$$\begin{aligned} I_{\text{p wave}}(\omega, \vec{k}) &\equiv I_{\text{p wave}, p}(\omega, \vec{k}) + I_{\text{p wave}, n}(\omega, \vec{k}) \\ &= - \int \frac{2d^3\vec{p}}{(2\pi)^3} \frac{\bar{E}_+(s, m_N^2, k^2)}{2\sqrt{m_N^2 + \vec{p}^2}} Q^2(s, m_N^2, k^2) \\ &\quad \times \left\{ \frac{1}{2} [F_P^{(0)}(s) + F_P^{(1)}(s)] n_p(\vec{p}) \right. \\ &\quad \left. + F_P^{(1)}(s) n_n(\vec{p}) \right\}, \quad (14) \end{aligned}$$

where $n_i(\vec{p})$ are the nucleon Fermi occupations, $i = (n, p)$. At zero temperature $n_p(\vec{p}) = \theta(p_{F,p} - |\vec{p}|)$ and $n_n(\vec{p}) = \theta(p_{F,n} - |\vec{p}|)$, $s = (\omega + \sqrt{m_N^2 + \vec{p}^2})^2 - (\vec{k} + \vec{p})^2$.

There are simple relations between the causal (“-”, “-”) and the retarded (“R”) Green's functions and polarization operators. For zero temperature and positive frequencies, they coincide. For $T \neq 0$ their real parts are still the same, whereas the imaginary parts are different, but can be interrelated. Bearing this in mind, we will further suppress the subscripts R and C for brevity.

Exploiting decomposition (9) of the p -wave scattering amplitude, we write

$$I_{\text{p wave}}(\omega, \vec{k}) = I_{\text{p wave}}^{\text{pole}}(\omega, \vec{k}) + I_{\text{p wave}}^{\text{reg}}(\omega, \vec{k}), \quad (15)$$

as the sum of the pole and the regular parts. The pole part is generated by hyperon exchanges

$$\begin{aligned} I_{\text{p-pole}}^{\text{pole}}(\omega, \vec{k}) &= I_{\Lambda}^{\text{pole}}(\omega, \vec{k}) + I_{\Sigma}^{\text{pole}}(\omega, \vec{k}) + I_{\Sigma^*}^{\text{pole}}(\omega, \vec{k}), \\ I_{\Lambda}^{\text{pole}}(\omega, \vec{k}) &= -C_{KN\Lambda}^2 \int \frac{2d^3\vec{p}}{(2\pi)^3} \frac{\bar{E}_-(m_{\Lambda}^2, m_N^2, k^2)}{\sqrt{m_N^2 + \vec{p}^2}} \\ &\quad \times \frac{(m_{\Lambda} + m_N)^2 m_{\Lambda}}{s^2 - m_{\Lambda}^2 + i0} n_p(\vec{p}), \quad (16) \end{aligned}$$

$$\begin{aligned} I_{\Sigma}^{\text{pole}}(\omega, \vec{k}) &= -C_{KN\Sigma}^2 \int \frac{2d^3\vec{p}}{(2\pi)^3} \frac{\bar{E}_-(m_{\Sigma}^2, m_N^2, k^2)}{\sqrt{m_N^2 + \vec{p}^2}} \\ &\quad \times \frac{(m_{\Sigma} + m_N)^2 m_{\Sigma}}{s^2 - m_{\Sigma}^2 + i0} [n_p(\vec{p}) + 2n_n(\vec{p})], \quad (17) \end{aligned}$$

$$\begin{aligned} I_{\Sigma^*}^{\text{pole}}(\omega, \vec{k}) &= -\frac{4}{3} C_{KN\Sigma^*}^2 \\ &\quad \times \int \frac{2d^3\vec{p}}{(2\pi)^3} \frac{\bar{E}_+(m_{\Sigma^*}^2, m_N^2, k^2)}{2\sqrt{m_N^2 + \vec{p}^2}} \frac{s}{m_{\Sigma^*}} \\ &\quad \times \frac{Q^2(s, m_N^2, k^2)}{s - m_{\Sigma^*}^2 + \frac{i}{2} \gamma_{\Sigma^*}(s)} [n_p(\vec{p}) + 2n_n(\vec{p})]. \quad (18) \end{aligned}$$

The regular part $I_{\text{p wave}}^{\text{reg}}$ can be expressed as

$$I_{\text{p wave}}^{\text{reg}}(\omega, \vec{k}) = \bar{I}_{\text{p wave}}^{\text{reg}}(\omega, \vec{k}) + \delta I_{\text{p wave}}^{\text{reg}}(\omega, \vec{k}), \quad (19)$$

including the part of integral (14) evaluated with $\delta F_P^{(1)}$ from Eq. (9),

$$\begin{aligned} \bar{I}_{\text{p wave}}^{\text{reg}}(\omega, \vec{k}) &= - \int \frac{2d^3\vec{p}}{(2\pi)^3} \frac{\bar{E}_+(s, m_N^2, k^2)}{2\sqrt{m_N^2 + \vec{p}^2}} Q^2(s, m_N^2, k^2) \\ &\quad \times \left\{ \frac{1}{2} [\delta F_P^{(0)}(s) + \delta F_P^{(1)}(s)] n_p(\vec{p}) \right. \\ &\quad \left. + \delta F_P^{(1)}(s) n_n(\vec{p}) \right\}, \quad (20) \end{aligned}$$

and the nonpole contributions from the hyperon exchanges

$$\delta I_{\text{p wave}}^{\text{reg}}(\omega, \vec{k}) = \delta I_{\Lambda}(\omega, \vec{k}) + \delta I_{\Sigma}(\omega, \vec{k}), \quad (21)$$

$$\begin{aligned} \delta I_{\Lambda}(\omega, \vec{k}) &= -C_{KN\Lambda}^2 \int \frac{2d^3\vec{p}}{(2\pi)^3} \\ &\quad \times \frac{m_{\Lambda} \sqrt{s - m_N^2 + k^2}}{2\sqrt{s} \sqrt{m_N^2 + \vec{p}^2}} \frac{(m_{\Lambda} + m_N)^2}{\sqrt{s + m_{\Lambda}}} n_p(\vec{p}), \quad (22) \end{aligned}$$

$$\begin{aligned} \delta I_{\Sigma}(\omega, \vec{k}) &= -C_{KN\Lambda}^2 \\ &\times \int \frac{2d^3\vec{p}}{(2\pi)^3} \frac{m_{\Sigma} \sqrt{s - m_N^2 + k^2}}{2\sqrt{s} \sqrt{m_N^2 + \vec{p}^2}} \\ &\times \frac{(m_{\Sigma} + m_N)^2}{\sqrt{s} + m_{\Sigma}} [n_p(\vec{p}) + 2n_n(\vec{p})]. \end{aligned} \quad (23)$$

To obtain the last relation, we used

$$\begin{aligned} \bar{E}(s, m_N^2, k^2) - \bar{E}(m_H^2, m_N^2, k^2) \\ = \frac{m_H \sqrt{s - m_N^2 + k^2}}{2m_H \sqrt{s}} (\sqrt{s} - m_H), \quad H = \{\Lambda, \Sigma\}. \end{aligned} \quad (24)$$

The above construction of the polarization operator corresponds to a gas approximation, and does not take into account either the mean-field potentials acting on baryons or the vertex corrections due to baryon-baryon correlations, or possible modifications of the scattering amplitudes in medium. The modification of the baryon propagator on the mean-field level can be easily incorporated in integrals (13) and (14) by the replacement $m_N \rightarrow m_N^*$. Effects induced by this modification in the kinematic prefactors in Eq. (13) and (14) can be easily traced back. The scaling of the nucleon mass in s is a more subtle issue. Solving the coupled-channel Bethe-Salpeter equation, one sums all two-particle reducible diagrams for the part of the s plane corresponding to a K^-N scattering. This approach is explicitly crossing noninvariant and a continuation of amplitudes far below the K^-N threshold can generate artificial singularities in the scattering amplitude. In Ref. [16], from where we borrow the amplitudes, the approximation scheme for solution of the Bethe-Salpeter equation was furnished in such a way that the K^-N and K^+N scattering amplitudes exhibit the *approximate crossing* symmetry, smoothly matching each other for $\sqrt{s} \sim m_N$. Therefore, amplitudes depicted in Figs. 2 and 3 are still physically well constrained in the corresponding intervals of \sqrt{s} shown there. However, for somewhat smaller \sqrt{s} , the K^-N s -wave scattering amplitude gets unphysical poles. To cure this problem, the complete solution of the Bethe-Salpeter equation for K^-N scattering has to be redone with medium modified baryon masses. Fortunately, there are some indications that this would not drastically change the results. We demonstrate here that the final results for integrals with the s -wave scattering amplitudes can be nicely modeled with the polarization operator following from a leading-order chiral Lagrangian, which has no explicit dependence on the baryon masses. Loop corrections due to the iteration of the interaction kernel should be suppressed for small kaon frequencies to keep the approximate crossing invariance of the amplitude. The pole subtracted p -wave amplitude is a rather smooth function of \sqrt{s} , as it is shown in Fig. 3, being mainly determined by the contact terms of the chiral Lagrangian and thus, has a weak baryon mass dependence. Hence, extrapolating the amplitude to somewhat smaller \sqrt{s} , we do not expect its strong variation. On contrary, the part of the po-

larization operator generated by the hyperon poles I_p^{pole} depends strongly on baryonic mean fields, which change the pole positions in the amplitude. This part will be treated explicitly in the course of our consideration.

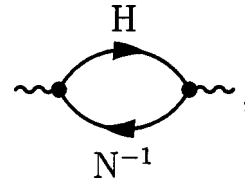
B. Pole part of the polarization operator

Here, we find the contributions to the K^- polarization operator from hyperon poles in the K^-N scattering amplitude determined by Eqs. (16)–(18). Relying on the explicit calculations of Refs. [6,15] we can easily incorporate the scalar and vector mean fields acting on baryons. The scalar field is taken into account with the help of the replacement $m_B \rightarrow m_B^*$. The baryon vector potentials are included in the pole terms by the shift of the kaon frequency $\omega \rightarrow \omega + \delta v_{iH}$, with $\delta v_{iH} = V_i - V_H$, $i = \{n, p\}$, $H = \{\Lambda, \Sigma\}$. This follows from the difference of the baryon energies, see Eq. (3). Please notice that this energy shift is obvious only for the pole contribution to the polarization operator. Generally, due to the absence of the gauge invariance for massive vector fields, such a shift is not motivated for more complicated diagrams.

Writing explicitly all contributions, we cast

$$\begin{aligned} \Pi^{(\text{pole},0)}(\omega, \vec{k}) &\equiv I_{p \text{ wave}}^{\text{pole}}(\omega, \vec{k}) \\ &= \Pi_{p\Lambda}^{(\text{pole},0)}(\omega, \vec{k}) + \Pi_{p\Sigma^0}^{(\text{pole},0)}(\omega, \vec{k}) \\ &\quad + 2\Pi_{n\Sigma^-}^{(\text{pole},0)}(\omega, \vec{k}) + \Pi_{p\Sigma^*0}^{(\text{pole},0)}(\omega, \vec{k}) \\ &\quad + 2\Pi_{n\Sigma^*-}^{(\text{pole},0)}(\omega, \vec{k}), \end{aligned} \quad (25)$$

where each term is equivalent to the pole contribution of the hyperon particle-nucleon-hole loop diagram (Schrödinger picture)



(26)

written in terms of the Lindhard function¹ as

$$\begin{aligned} \Pi_{iH}^{(\text{pole},0)}(\omega, \vec{k}) &= C_{KNH}^2 [(m_H^* - m_N^*)^2 - (\omega + \delta v_{iH})^2 \\ &\quad + \vec{k}^2] \eta_{NH}^2 \Phi_{iH}(\omega, \vec{k}), \end{aligned}$$

$$\Pi_{i\Sigma^*}^{(\text{pole},0)}(\omega, \vec{k}) = C_{KN\Sigma^*}^2 \eta_{i\Sigma^*}^2 (\omega, \vec{k}) \vec{k}^2 \Phi_{i\Sigma^*}(\omega, \vec{k}),$$

$$\eta_{NH} = \frac{m_N^* + m_H^*}{2m_N^*},$$

¹For further convenience, we introduce notation $i = (n, p)$ and continue to use N when the quantity does not depend on the nucleon isospin.

$$\eta_{i\Sigma^*}^2(\omega, \vec{k}) = \frac{(m_{\Sigma^*}^* + m_N^*)^2 - (\omega + \delta v_{iH})^2 + \vec{k}^2}{6m_{\Sigma^*}^{*2}}. \quad (27)$$

We reserved the superscript ‘‘0’’ for each term in Eq. (25) to indicate that neither the baryon self-energy corrections beyond a mean-field approximation nor the vertex corrections due to baryon-baryon correlations are included. The (retarded) Lindhard function Φ accounting for the relativistic kinematics is defined as

$$\Phi_{iH}(\omega, \vec{k}) = \int \frac{2d^3p}{(2\pi)^3 2\epsilon_i(p)} \frac{4m_N^{*2}}{s - m_H^2 + i0} n_i(\vec{p}). \quad (28)$$

For zero temperature, we have

$$\Phi_{iH}(\omega, \vec{k}) = \frac{m_N^{*2}}{2\pi^2 |\vec{k}|} \int_0^{p_{Fi}} \frac{dpp}{\epsilon_i(p)} \ln \left[\frac{\Delta_{iH}^+(\omega, \vec{k}, \vec{p})}{\Delta_{iH}^-(\omega, \vec{k}, \vec{p})} \right],$$

$$\Delta_{iH}^\pm(\omega, \vec{k}, \vec{p}) = [\omega + \delta v_{iH} + \epsilon_i(\vec{p})]^2 - \epsilon_H^2(|\vec{p}| \mp |\vec{k}|), \quad (29)$$

where p_{Fi} is the Fermi momentum of the nucleon species i . The nonrelativistic form of the Lindhard function used, e.g., in Ref. [21] (with a different normalization) is recovered after expanding $\epsilon_B(p) \approx m_B^* + p^2/(2m_B^*)$ in Eq. (29).

The imaginary part of the (retarded) Lindhard function is obtained as an analytical continuation $\ln(x) = \ln|x| + i\pi\theta(-x)$ leading to nonzero contribution for

$$\omega_{iH}^-(\vec{k}) < \omega < \omega_{iH}^+(\vec{k}). \quad (30)$$

Here, ω_{iH}^\pm are the upper and the lower borders of the corresponding particle-hole continuum

$$\omega_{iH}^+(\vec{k}) = \begin{cases} \sqrt{(m_H^* - m_N^*)^2 + \vec{k}^2} + \delta v_{iH}, & k < p_{Fi} \left(\frac{m_H^*}{m_N^*} - 1 \right) \\ E_H(|\vec{k}| + p_{Fi}) - E_i(p_{Fi}), & k > p_{Fi} \left(\frac{m_H^*}{m_N^*} - 1 \right), \end{cases} \quad (31)$$

$$\omega_{iH}^-(\vec{k}) = E_H(|\vec{k}| - p_{Fi}) - E_i(p_{Fi}). \quad (32)$$

Baryon energies include vector potentials according to Eq. (3).

An approximate expression for Φ_{iH} renders

$$\Phi_{iH}(\omega, \vec{k}) \approx - \frac{m_N^{*2}}{8\pi^2 |\vec{k}|^3 \epsilon_{Fi}} \left[\frac{\tilde{\Delta}_{iH}^+ \tilde{\Delta}_{iH}^-}{2} \ln \left(\frac{\tilde{\Delta}_{iH}^+}{\tilde{\Delta}_{iH}^-} \right) - \frac{(\tilde{\Delta}_{iH}^+)^2 - (\tilde{\Delta}_{iH}^-)^2}{4} \right],$$

with $\tilde{\Delta}_{iH}^\pm = \Delta_{iH}^\pm(\omega, \vec{k}, p_{Fi})$ and $\epsilon_{Fi} = \epsilon_i(p_{Fi})$, being valid for $\omega < (\omega_{iH}^+ + \omega_{iH}^-)/2$.

V. *s*- AND *p*-WAVE PARTS OF THE POLARIZATION OPERATOR

In our discussion, we would like to put particular emphasis on in-medium effects, which modify the K^- spectrum at finite momenta. For this purpose, we define the momentum independent part, called the *s*-wave part of the polarization operator, and the momentum dependent part, called the *p*-wave part of the polarization operator:

$$\begin{aligned} \Pi_C^{(0)}(\omega, \vec{k}) &= \Pi_S^{(0)}(\omega) + \Pi_P^{(0)}(\omega, \vec{k}) \\ &\equiv \Pi_C^{(0)}(\omega, 0) + [\Pi_C^{(0)}(\omega, \vec{k}) - \Pi_C^{(0)}(\omega, 0)]. \end{aligned}$$

The term $\Pi_C^{(0)}(\omega, 0)$ does not depend on \vec{k} , whereas the term $[\Pi_C^{(0)}(\omega, \vec{k}) - \Pi_C^{(0)}(\omega, 0)]$ depends on \vec{k} , and vanishes at $|\vec{k}| = 0$. In order to avoid misunderstanding, we point out that the *s*- and *p*-wave scattering amplitudes contribute to both parts of the polarization operator

$$\Pi_S^{(0)}(\omega) = I_{s\text{ wave}}(\omega, 0) + I_{p\text{ wave}}(\omega, 0),$$

$$\begin{aligned} \Pi_P^{(0)}(\omega, \vec{k}) &= [I_{s\text{ wave}}(\omega, \vec{k}) - I_{s\text{ wave}}(\omega, 0)] + [I_{p\text{ wave}}(\omega, \vec{k}) \\ &\quad - I_{p\text{ wave}}(\omega, 0)]. \end{aligned} \quad (33)$$

In the following, we discuss the *s*- and *p*-wave parts of the polarization operator.

A. *p*-wave part

Following decomposition (15), we split the *p*-wave part of the polarization operator into the pole and the regular contributions

$$\Pi_P^{(0)}(\omega, \vec{k}) = \Pi_P^{(\text{pole}, 0)}(\omega, \vec{k}) + \Pi_P^{(\text{reg}, 0)}(\omega, \vec{k}). \quad (34)$$

For the pole *p*-wave part, we have

$$\begin{aligned} \Pi_P^{(\text{pole}, 0)}(\omega, \vec{k}) &= I_P^{(\text{pole})}(\omega, \vec{k}) - I_P^{(\text{pole})}(\omega, 0) \\ &= \Pi_{p\Lambda}^{(P, 0)}(\omega, \vec{k}) + \Pi_{p\Sigma^0}^{(P, 0)}(\omega, \vec{k}) + 2\Pi_{n\Sigma^-}^{(P, 0)}(\omega, \vec{k}) \\ &\quad + \Pi_{p\Sigma^*0}^{(P, 0)}(\omega, \vec{k}) + 2\Pi_{n\Sigma^*-}^{(P, 0)}(\omega, \vec{k}), \end{aligned} \quad (35)$$

$$\Pi_{iH}^{(P, 0)}(\omega, \vec{k}) = \Pi_{iH}^{(\text{pole}, 0)}(\omega, \vec{k}) - \Pi_{iH}^{(\text{pole}, 0)}(\omega, 0), \quad (36)$$

where we used Eqs. (16)–(18) and (25).

Expanding the *p*-wave pole part of the polarization operator for small kaon momenta, we have

$$\begin{aligned} \Pi_{iH}^{(P, 0)}(\omega, \vec{k}) &= C_{KNH}^2 \vec{k}^2 \phi_{iH}^P(\omega) + O(\vec{k}^4), \\ \phi_{iH}^P(\omega) &= \eta_{NH}^2 \Phi_{iH}(\omega, 0) + \eta_{NH}^2 [(m_H^* - m_N^*)^2 \\ &\quad - (\omega + \delta v_{iH})^2] \frac{\partial \Phi_{iH}(\omega, \vec{k})}{\partial \vec{k}^2} \Big|_{|\vec{k}|=0}, \end{aligned} \quad (37)$$

$$\Phi_{i\Sigma^*}(\omega, \vec{k}) = C_{KN\Sigma^*}^2 \vec{k}^2 \eta_{i\Sigma^*}^2(\omega, 0) \Phi_{i\Sigma^*}(\omega, 0). \quad (38)$$

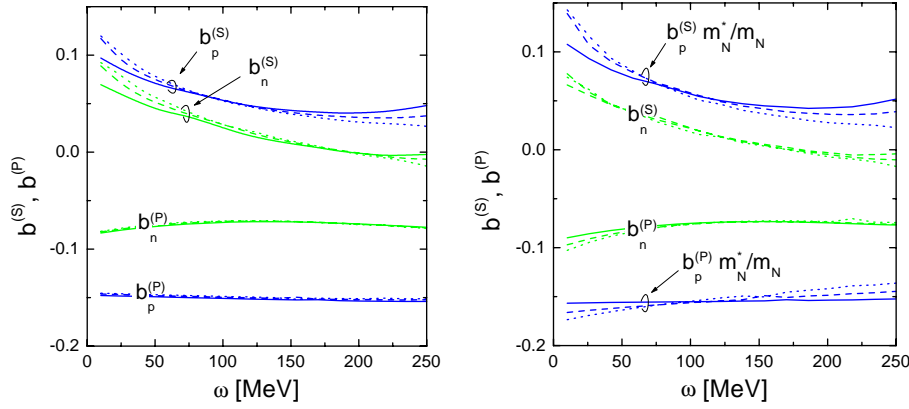


FIG. 4. Left panel: Coefficients (40) of expansion (39) of the polarization operator. Solid, dashed, and dotted lines correspond to nucleon densities $\rho_{n,p} = 1\rho_0, 3\rho_0,$ and $5\rho_0$, respectively. Right panel: the same as on the left plane but integrals evaluated with effective nucleon mass in kinematical prefactors and coefficients $b_p^{(S,P)}$ scaled by m_N^*/m_N .

The regular part of the p -wave polarization operator is defined by

$$\Pi_p^{(\text{reg},0)}(\omega, \vec{k}) = [I_{s \text{ wave}}(\omega, \vec{k}) - I_{s \text{ wave}}(\omega, 0)] + [I_{p \text{ wave}}^{\text{reg}}(\omega, \vec{k}) - I_{p \text{ wave}}^{\text{reg}}(\omega, 0)].$$

At small kaon momenta, the real part of $\Pi_p^{(\text{reg},0)}$ can be written as

$$\text{Re}\Pi_p^{(\text{reg},0)}(\omega, \vec{k}) = \vec{k}^2 \left(b_p(\omega) \frac{\rho_p}{\rho_0} + b_n(\omega) \frac{\rho_n}{\rho_0} \right) + O(k^4), \quad (39)$$

$$b_i(\omega) = b_i^{(S)}(\omega) + b_i^{(P)}(\omega),$$

$$b_i^{(S)}(\omega) = \left. \frac{\rho_0}{\rho_i} \frac{\partial}{\partial \vec{k}^2} I_{s \text{ wave},i}(\omega, \vec{k}) \right|_{\vec{k}=0},$$

$$b_i^{(P)}(\omega) = \left. \frac{\rho_0}{\rho_i} \frac{\partial}{\partial \vec{k}^2} I_{p \text{ wave},i}^{\text{reg}}(\omega, \vec{k}) \right|_{\vec{k}=0}, \quad (40)$$

where we used the fact that the real part of the kaon polarization operator is an even function of the kaon momentum.

The quantities $b_n^{(S,P)}$ and $b_p^{(S,P)}$ are shown in Fig. 4 for $T=0$ and for several values of densities ρ_i as functions of the kaon energy.

In these calculations, the integrals I_s and I_p have been evaluated with the free nucleon masses. We see that these coefficients are almost density independent and only weakly dependent on the kaon energy in the interval $100 \text{ MeV} < \omega < 250 \text{ MeV}$. As we have discussed in the beginning of this section, we replace the baryon masses by the effective masses, as they follow from the mean-field solutions, only in the kinematical prefactors in Eqs. (13) and (14). The results are shown in the right plane of Fig. 4. The coefficients $b_n^{(S,P)}$ depend moderately on the density whereas the coefficients $b_p^{(S,P)}$ exhibit a stronger density dependence, which can be parametrized by the factor m_N/m_N^* as demonstrated in Fig. 4. The energy dependence is still weak in the $100 \text{ MeV} < \omega < 250 \text{ MeV}$ interval.

Our result (39) is derived for rather small values of a kaon momentum, $|\vec{k}| \ll m_K$. In order to find the actual value of the

p -wave K^- condensate amplitude in the most general case, one needs to deal with momenta up to $|\vec{k}| \sim p_{F,n} \sim m_K$. In this case, we have to extrapolate our result for the regular part of the polarization operator to such momenta. Fortunately, within our approach the critical points of the s - and p -wave condensations do not deviate much from each other and the kaon condensate momentum in the vicinity of the critical density remains small. Also, the main contribution to the kaon polarization operator comes from the pole terms, which are written explicitly for arbitrary momenta in Eq. (25). Thereby, the ambiguity of the mentioned interpolation should not significantly affect our conclusions.

B. s -wave part

The kaon-nucleon interaction results in the following contributions to the s -wave part of the K^- meson polarization operator

$$\Pi_S^{(0)}(\omega) = I_{s \text{ wave}}(\omega, 0) + \bar{I}_{p \text{ wave}}^{\text{reg}}(\omega, 0) + \delta\Pi^{(\text{reg},0)}(\omega) + \Pi^{(\text{pole},0)}(\omega, 0), \quad (41)$$

where the last two terms correspond to nonpole and pole parts of the hyperon exchange terms in the amplitude, respectively. The $\Pi^{(\text{pole},0)}$ term is given by Eq. (25). Using Eq. (21), we present $\delta\Pi^{(\text{reg},0)}$ as follows:

$$\begin{aligned} \delta\Pi^{(\text{reg},0)}(\omega) &\equiv \delta I_{p \text{ wave}}^{\text{reg}}(\omega, 0) \\ &= \delta\Pi_{p\Lambda}^{(\text{reg},0)}(\omega, 0) \\ &\quad + \delta\Pi_{p\Sigma^0}^{(\text{reg},0)}(\omega, 0) + 2\delta\Pi_{n\Sigma^-}^{(\text{reg},0)}(\omega, 0), \end{aligned}$$

with

$$\begin{aligned} \delta\Pi_{iH}^{(\text{reg},0)}(\omega, 0) &= -C_{KNH}^2 \int \frac{2d^3\vec{p}}{(2\pi)^3} \\ &\quad \times \frac{(m_H^* \sqrt{s_0} - m_N^{*2} + \omega^2)(m_H^* + m_N^*)^2}{2\epsilon_i(p) \sqrt{s_0}(\sqrt{s_0} + m_H^*)} n_i(\vec{p}), \end{aligned} \quad (42)$$

where $s_0 = [\omega + \epsilon_i(\vec{p})]^2 - \vec{p}^2$. We also included the dependence of the effective masses on the mean field. For $T=0$

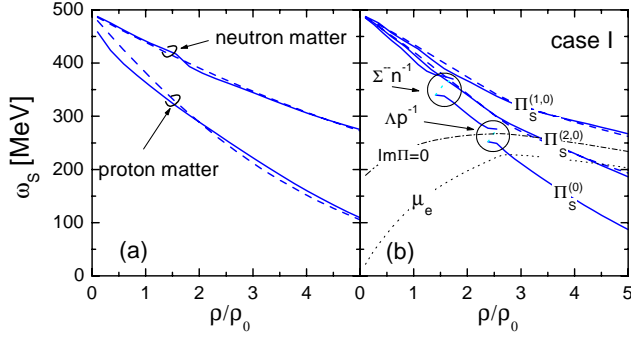


FIG. 5. Panel (a): The energy of the lowest K^- branch of the dispersion equation (45) at $\vec{k}=0$ calculated with $\Pi_S^{(1,0)}$ (solid lines) for proton and neutron matter. Dashed lines present approximate spectra given by Eq. (49). Panel (b): The energy of the lowest K^- branch of Eq. (45) at $\vec{k}=0$ for neutron star matter (case I of the hyperon-nucleon interaction) corresponding to the s -wave polarization operators $\Pi_S^{(1,0)}$, $\Pi_S^{(2,0)}$, $\Pi_S^{(0)}$ given by Eqs. (46)–(48) (solid lines). Dashed lines are solutions for approximate relations (43) and (50). Dotted line shows the electron chemical potential. Dash-dotted line depicts the border of the imaginary part of the K^- polarization operator (border of hyperonization).

and for small kaon energies the integral in Eq. (42) can be well approximated by the following expression:

$$\delta\Pi_{iH}^{(\text{reg},0)}(\omega,0) \approx -C_{KNH}^2 \left(\frac{m_H^{*2} - m_N^{*2}}{2m_N^*} \rho_i^{\text{scal}} + \omega \rho_i - \frac{\omega^2}{m_H^* + m_N^*} \rho_i \right), \quad (43)$$

where ρ_i^{scal} stands for the scalar density of nucleons defined by

$$\rho_i^{\text{scal}} = \int_0^{p_{F,i}} \frac{2d^3\vec{p}}{(2\pi)^3} \frac{m_N^*}{\epsilon_i(\vec{p})}. \quad (44)$$

C. Energy of the lowest branch of the dispersion equation at $\vec{k}=0$

In this section, we illustrate the strength of the different terms in Eq. (41), applying the polarization operator to the problem of the s -wave kaon condensation.

Neutron star matter becomes unstable with respect to reactions (1) producing K^- mesons at the zero momentum when the solution [$\omega_S = \omega^{\min}(\vec{k})$ at $\vec{k}=0$] of the dispersion equation

$$\omega_S^2 - m_K^2 - \text{Re}\Pi_S(\omega_S) = 0, \quad (45)$$

related to the lowest branch of the spectrum, meets the electron chemical potential. Then, the s -wave K^- condensation may occur via a second-order phase transition.

In Fig. 5, we present the energy of the lowest K^- branch of the dispersion equation (45) with momentum $\vec{k}=0$ as a function of the density. The hyperon interactions are taken

according to case I. In order to illustrate the strength of different contributions to the s -wave part of the polarization operator (41), we consider several test polarization operators

$$\Pi_S^{(1,0)}(\omega) = I_{s\text{ wave}}(\omega,0) + \bar{I}_{p\text{ wave}}^{\text{reg}}(\omega,0), \quad (46)$$

$$\Pi_S^{(2,0)}(\omega) = \Pi_S^{(1,0)}(\omega) + \delta\Pi^{(\text{reg},0)}(\omega), \quad (47)$$

$$\Pi_S^{(0)}(\omega) = \Pi_S^{(2,0)}(\omega) + \Pi^{(\text{pole},0)}(\omega,0). \quad (48)$$

In Fig. 5(a) solid lines show the energy of the lowest branch of the solution of Eq. (45) with $\Pi_S^{(1,0)}$ for the cases of pure proton and neutron matter. The contribution of $\bar{I}_{p\text{ wave}}^{\text{reg}}(\omega,0)$ is very small, at the level of few percent. It is instructive to compare this result with the one given by the frequently used parametrization of the K^- spectrum motivated by the leading-order chiral perturbation theory (χ PT) [8],

$$\omega_S^{\chi\text{PT}}(\rho_n, \rho_p) = \sqrt{m_K^2 - S_K + V_K^2} - V_K,$$

$$S_K = \frac{1}{f^2} [\Sigma_{KN}(\rho_p^{\text{scal}} + \rho_n^{\text{scal}}) + C(\rho_p^{\text{scal}} - \rho_n^{\text{scal}})],$$

$$V_K = \frac{(2\rho_p + \rho_n)}{4f^2}, \quad (49)$$

where $f \approx 90$ MeV is the pion decay constant in the chiral limit [16], and Σ_{KN} and C stand for the isoscalar and the isovector kaon-nucleon Σ terms, and are related to explicit chiral symmetry breaking. The SU(3) symmetry predicts $C = m_K^2(2m_\Xi - 3m_\Sigma + m_\Lambda)/[16(m_K^2 - m_\pi^2)] \approx 66$ MeV [4]. A model polarization operator leading to the dispersion relation (49) can be written as [8]

$$\Pi_S^{(\chi\text{PT},0)}(\omega) = -\frac{\Sigma_{KN}}{f^2}(\rho_p^{\text{scal}} + \rho_n^{\text{scal}}) - \frac{C}{f^2}(\rho_p^{\text{scal}} - \rho_n^{\text{scal}}) - \frac{2\rho_p + \rho_n}{2f^2}\omega. \quad (50)$$

Spectrum (49), calculated using $\Sigma_{KN} = 150$ MeV, is shown in Fig. 5 [panel (a)] by dashed lines. We observe a good agreement of the model spectrum with the one following from the numerical evaluation of the integrals [$I_{s\text{ wave}}(\omega,0) + \bar{I}_{p\text{ wave}}^{\text{reg}}(\omega,0)$]. The obtained value of the effective kaon-nucleon Σ term is two to three times smaller than what was used as an *ad hoc* parameter in Ref. [8] with the same parametrization (50).

The results for the realistic composition of neutron star matter (Fig. 1, case I) are presented in Fig. 5(b) as a representative example. Solid lines depict the energy of the lowest branch of the dispersion equation calculated for $\vec{k}=0$ with $\Pi_S^{(1,0)}$, $\Pi_S^{(2,0)}$, and $\Pi_S^{(0)}$. Dashed lines show solutions obtained with the approximate expressions (50) in $\Pi_S^{(1,0)}$ and (43) for $\delta\Pi^{(\text{reg},0)}$ in $\Pi_S^{(2,0)}$. The excellent coincidence of the curves justifies the accuracy of Eqs. (50) and (43).

The crossing point of the solid and dotted lines corresponds to the critical density of the s -wave condensation. We observe that the lines corresponding to $\Pi_S^{(1,0)}$ do not cross the chemical potential (dotted line). Therefore, the s -wave kaon-nucleon interaction, following from Ref. [16], would not support a second-order phase transition into the s -wave K^- condensate state due to the small value of the kaon-nucleon Σ term. However, an additional attraction comes from the term $\delta I_{p\text{ wave}}^{(\text{reg})}$ included in $\Pi_S^{(2,0)}$. It makes the condensation possible at densities $\geq 4.5\rho_0$. Another attractive piece is the pole term $I_{p\text{ wave}}^{\text{pole}}(\omega, 0)$ taken into account in $\Pi_S^{(0)}$. The significance of these terms, originating both from the hyperon exchange diagram in $\bar{K}N$ interaction, was pointed first in Ref. [6]. Both of these contributions were disregarded in works [8,9,5,7,10–12] discussing the s -wave K^- condensation.

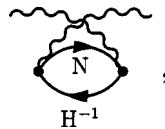
The curves ω_S calculated with the full s -wave polarization operator $\Pi_S^{(0)}$ have cuts. In the region between the cuts, Eq. (45) has no solutions with positive residues [6]. The dashed-dotted line depicts the border of the imaginary part of the K^- polarization operator. We see that within our approach, the curve calculated with $\Pi_S^{(0)}$ and μ_e meet at an energy below the region of the imaginary part. Thus, with the full polarization operator (41) and (48), we recovered the results of previous works [8,9,5,7,10–12] (where, however, the two to three times larger Σ term was used) about the possibility of the K^- condensate production in reaction (1) at rather moderate densities. In our case, the critical density is $\rho_{c,S} \approx 2.7\rho_0$. The reader should bear in mind that the baryon-baryon correlations are still not included in the above analysis. They will increase $\rho_{c,S}$. This issue is addressed in Sec. VII.

VI. CONTRIBUTIONS OF THE HYPERON FERMI SEAS TO THE POLARIZATION OPERATOR

When the nucleon density exceeds the critical density of hyperonization $\rho_{c,H}$, the Fermi sea of hyperon H begins to grow, and the K^- polarization operator receives new contributions.

A. Pole terms

The hyperon contribution to the K^- polarization operator is related to the diagrams (in Schrödinger picture)



(51)

where hyperons and nucleons interchange their roles compared to diagram (26).

The hyperon contributions to the pole part of the polarization operator $\Pi^{(\text{pole},0)}$ can be simply included in Eq. (27) with the help of the replacement

$$\eta_{iH}^2 \Phi_{iH}(\omega, \vec{k}) \rightarrow \eta_{NH}^2 \Phi_{iH}(\omega, \vec{k}) + \eta_{HN}^2 \Phi_{Hi}(-\omega, -\vec{k}), \quad (52)$$

where the last term implies interchange of all indices $i \leftrightarrow H$ in Eqs. (28), (29), and (34). The result of such a replacement can be cast as

$$\begin{aligned} \delta \Pi_{\text{hyp}}^{(\text{pole},0)}(\omega, \vec{k}) &= \Pi_{\Lambda p}^{(\text{pole},0)}(-\omega, -\vec{k}) + \Pi_{\Sigma^0 p}^{(\text{pole},0)}(-\omega, -\vec{k}) \\ &\quad + 2\Pi_{\Sigma^- n}^{(\text{pole},0)}(-\omega, -\vec{k}), \end{aligned} \quad (53)$$

and is to be added to the total polarization operator.

B. Regular terms

There are no experimental constraints on the hyperon contribution to the regular part of the polarization operator. As a rough estimation, we suggest to extend the model polarization operator (50) to the hyperon sector according to the leading-order terms of a chiral Lagrangian

$$\begin{aligned} \delta \Pi_{S,\text{hyp}}^{(\chi\text{PT},0)}(\omega) &= -\frac{\Sigma_{KN}}{f^2} (\rho_{\Lambda}^{\text{scal}} + \rho_{\Sigma^-}^{\text{scal}} + \rho_{\Xi^-}^{\text{scal}}) - \frac{C}{f^2} \left(\frac{1}{3} \rho_{\Lambda}^{\text{scal}} \right. \\ &\quad \left. - \rho_{\Sigma^-}^{\text{scal}} + \rho_{\Xi^-}^{\text{scal}} \right) + \frac{C_{\Lambda}}{f^2} \rho_{\Lambda}^{\text{scal}} + \frac{\rho_{\Sigma^-} + 2\rho_{\Xi^-}}{2f^2} \omega. \end{aligned} \quad (54)$$

In this expression, we utilize the value of Σ_{KN} from the fit with formula (49) to the numerical results in Fig. 5 ($\Sigma_{KN} \approx 150$ MeV), whereas the values of coefficients $C \approx 66$ MeV and $C_{\Lambda} = m_K^2(m_{\Xi} - m_{\Lambda})/[12(m_K^2 - m_{\pi}^2)] \approx 34$ MeV and $f \approx 90$ MeV are predicted by the chiral SU(3) symmetry. To estimate the nonpole contribution from the nucleon u -channel exchange (analogous to $\delta \Pi^{(\text{reg},0)}$), we use the approximate relation (43)

$$\begin{aligned} \delta \Pi_{S,\text{hyp}}^{(\text{reg},0)}(\omega) &= -C_{KN\Lambda}^2 \left[\frac{m_N^{*2} - m_{\Lambda}^{*2}}{2m_{\Lambda}^*} \rho_{\Lambda}^{\text{scal}} - \omega \rho_{\Lambda} \right. \\ &\quad \left. - \frac{\omega^2}{m_{\Lambda}^* + m_N^*} \rho_{\Lambda} \right] - 2C_{KN\Sigma}^2 \left[\frac{m_N^{*2} - m_{\Sigma}^{*2}}{2m_{\Sigma}^*} \rho_{\Sigma^-}^{\text{scal}} \right. \\ &\quad \left. - \omega \rho_{\Sigma^-} - \frac{\omega^2}{m_{\Sigma}^* + m_N^*} \rho_{\Sigma^-} \right]. \end{aligned} \quad (55)$$

In our estimation, we do not take into account contributions to the regular p -wave part of the polarization operator $\propto \vec{k}^2 \rho_H$.

C. The energy of the lowest branch of the dispersion equation at $\vec{k}=0$

Solutions related to the lowest branch of the dispersion equation (45) for $\vec{k}=0$ calculated with the polarization operator

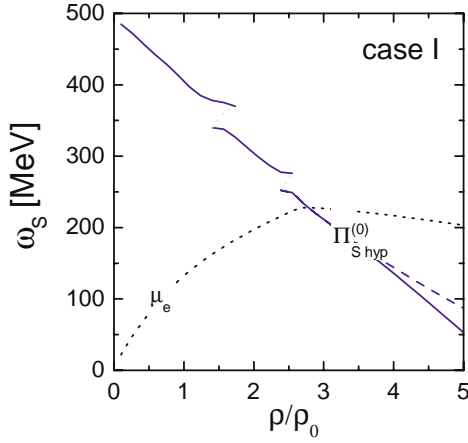


FIG. 6. The energy of the lowest branch of the dispersion equation at $\vec{k}=0$ calculated with the polarization operator $\Pi_{S,\text{hyp}}^{(0)}$ given by Eq. (56) is depicted by solid lines. The dashed line shows the corresponding solution with the polarization operator (48). The dotted line depicts the electron chemical potential.

$$\Pi_{S,\text{hyp}}^{(0)}(\omega) = \Pi_S^{(0)}(\omega) + \delta\Pi_{S,\text{hyp}}^{(0)}(\omega),$$

$$\delta\Pi_{S,\text{hyp}}^{(0)}(\omega) = \delta\Pi_{S,\text{hyp}}^{(\chi\text{PT},0)}(\omega) + \delta\Pi_{\text{hyp}}^{(\text{reg},0)}(\omega) + \delta\Pi_{\text{hyp}}^{(\text{pole},0)}(\omega, 0) \quad (56)$$

are shown in Fig. 6 by solid lines in comparison with the corresponding solutions obtained without inclusion of hyperons (dashed lines). Calculations are done for the hyperon coupling constants corresponding to case I. We see that the presence of hyperons produces an additional small attraction only at rather high densities ($>4\rho_0$). The net effect is small due to the partial cancellation of the attractive $\Pi_{S,\text{hyp}}^{(\chi\text{PT},0)}$ term and the repulsive $\delta\Pi_{\text{hyp}}^{(\text{reg},0)}$ term and because in our model the hyperon concentrations are much smaller than the neutron concentration and even smaller than the proton one. This allows us not to care much about the hyperon Fermi-sea occupations when considering the $\vec{k}=0$ case.

VII. BARYON-BARYON CORRELATIONS

Working with the polarization operator constructed by integrating the meson-nucleon scattering amplitude over the nucleon Fermi sea, e.g., as in Eqs. (13) and (14), one assumes that all multiple meson-nucleon interactions are independent from each other and have the same probability proportional to the local nucleon density $\rho(\vec{r})$. However, successive meson-nucleon scatterings in dense nuclear matter are not independent due to the presence of a repulsive core in nucleon-nucleon interactions, and due to the Pauli exclusion principle [46–48]. The probability to find two nucleons i and i' at the positions \vec{r}_1 and \vec{r}_2 , respectively, is proportional to the two-particle density

$$\rho_{ii'}(\vec{r}_1, \vec{r}_2) = [1 + C_{ii'}(|\vec{r}_1 - \vec{r}_2|)]\rho_i(\vec{r}_1)\rho_{i'}(\vec{r}_2),$$

with the correlation function $C_{ii'}(r) < 0$ and it is reduced in comparison to the product of two single-particle densities. The correlation function can be approximately written as

$$C_{ii'}(r) \approx C^{\text{core}}(r) + \delta_{ii'} C_i^{\text{Pauli}}(r) [1 + C^{\text{core}}(r)] \quad (57)$$

with contributions from the hard core, C^{core} , and the Pauli exclusion principle, C^{Pauli} , assuming that both correlations contribute multiplicatively. The former can be taken from the description of the nuclear matter with the realistic nucleon-nucleon interaction. A convenient parametrization $C^{\text{core}}(r) \approx -j_0(m_0 r)$ with $m_0 \approx 5.6m_\pi$ was suggested in Ref. [49]. Here, $j_l(x)$ is the spherical Bessel function. For the Pauli correlation, we use the expression for the ideal fermion gas [50], $C_i^{\text{Pauli}}(r) = -9j_1^2(p_{\text{Fi}} r)/(2p_{\text{Fi}}^2 r^2)$.

A. Correction of s -wave and regular p -wave terms

A general derivation of corrections to the meson propagation in dense nuclear matter due to nucleon-nucleon correlations (so-called Ericson-Ericson-Lorentz-Lorenz corrections) can be found in Refs. [51,52] for pions and in Refs. [53,54] for kaons.

Correlation processes can be presented by symbolic diagrammatic equation

$$\text{Diagram} = \text{Diagram} + \sum_{B'} \text{Diagram} \quad (58)$$

The wavy line represents the kaon, and the sum goes over baryon species. The absence of arrows on the solid fermion lines means that both particles and holes are treated on equal footing (the conservation of charges, e.g., strangeness, baryonic number, etc., in each vertex is implied). The hatched triangle is the bare scattering amplitude (scattering on a particle or on a hole) and the full triangle stands for the amplitude including baryon-baryon correlations. The dotted line symbolically depicts the two-baryon correlation function $C_{BB'}$ due to the BB' correlations through the core and the Pauli principle. There are neither experimental informations nor theoretical estimations for the hyperon-nucleon and hyperon-hyperon correlations. Since the latter ones are less relevant for our discussion below we will neglect them. Thus, we include only minimal correlations given by the $C_{ii'}$ nucleon-nucleon correlation functions.

First, we consider correlation corrections to the s -wave part of the kaon polarization operator $\Pi_S^{(0)}$ given by Eq. (41) and the regular p -wave part $\Pi_p^{(\text{reg},0)}$ from Eq. (39). We separate the contributions induced by the scattering on a nucleon species $i = \{n, p\}$

$$\Pi_S^{(0)}(\omega) = \Pi_{S,n}^{(0)}(\omega) + \Pi_{S,p}^{(0)}(\omega),$$

$$\Pi_{S,i}^{(0)}(\omega) = I_{s \text{ wave},i}(\omega, 0) + I_{p \text{ wave},i}(\omega, 0),$$

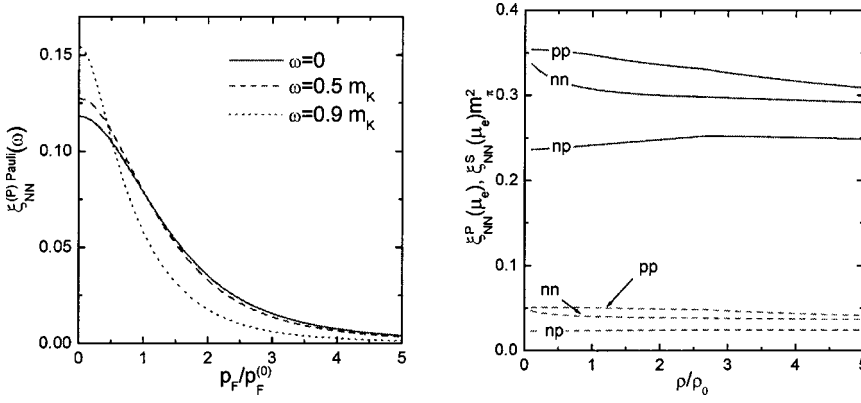


FIG. 7. Left panel—contribution for the Pauli spin correlations to the p -wave correlation function (62) vs the Fermi momentum for different kaon energies ($p_F^{(0)}$ is the Fermi momentum for $\rho = \rho_0$); Right panel—the s -wave (dashed lines) and p -wave (solid lines) correlation functions (61) and (62) evaluated for $\omega = \mu_e$ in neutron star matter (case I) as function of the total baryon density.

cf. Eqs. (13) and (14). Then, adopting results from Refs. [55,54], we may present the polarization operator terms corrected by baryon-baryon correlations as

$$\Pi_S(\omega) = \frac{\tilde{\Pi}_{S,n}(\omega) + \tilde{\Pi}_{S,p}(\omega) + 2\tilde{\Pi}_{S,n}(\omega)\tilde{\Pi}_{S,p}(\omega)\xi_{pn}^{(S)}(\omega)}{1 - \tilde{\Pi}_{S,n}(\omega)\tilde{\Pi}_{S,p}(\omega)(\xi_{pn}^{(S)}(\omega))^2},$$

$$\tilde{\Pi}_{S,i}(\omega) = \frac{\Pi_{S,i}^{(0)}(\omega)}{1 - \xi_{ii}^{(S)}(\omega)\Pi_{S,i}^{(0)}(\omega)}, \quad (59)$$

$$\Pi_P^{\text{reg}}(\omega, \vec{k}) = k^2 \frac{\tilde{b}_p(\omega) + \tilde{b}_n(\omega) + 2\tilde{b}_p(\omega)\tilde{b}_n(\omega)\xi_{np}^{(P)}(\omega)}{1 - \tilde{b}_p(\omega)\tilde{b}_n(\omega)(\xi_{np}^{(P)}(\omega))^2},$$

$$\tilde{b}_i(\omega) = \frac{b_i(\omega)(\rho_i/\rho_0)}{1 - b_i(\omega)\rho_i\xi_{ii}^{(P)}(\omega)/\rho_0}. \quad (60)$$

The functions $\xi_{ii'}^{(S)}$ and $\xi_{ii'}^{(P)}$ are defined as

$$\xi_{ii'}^{(S)}(\omega) = \int d^3r C_{ii'}(r) D_K^0(\omega, r), \quad (61)$$

$$\xi_{ii'}^{(P)}(\omega) = \frac{1}{3} \int d^3r C_{ii'}(r) \nabla^2 D_K^0(\omega, r)$$

$$= -\frac{1}{3} [C_{ii'}(0) - (m_K^2 - \omega^2)\xi_{ii'}^{(S)}(\omega)], \quad (62)$$

with the Pauli and hard-core contributions from Eq. (57), $i, i' = \{n, p\}$, and $D_K^0(\omega, r) = -\exp(-\sqrt{m_K^2 - \omega^2}r)/(4\pi r)$ as the free kaon propagator.

Using Eq. (58), one finds that the repulsive core contributes with

$$\xi_{ii'}^{(P, \text{core})} = \xi_K^{(P, \text{core})}(\omega) = \frac{1}{3} \frac{m_0^2}{(m_0^2 + m_K^2 - \omega^2)} \quad (63)$$

to the p wave ξ 's and with

$$\xi_{ii'}^{(S, \text{core})} = \xi_K^{(S, \text{core})}(\omega) = \frac{1}{(m_0^2 + m_K^2 - \omega^2)} \quad (64)$$

to the s -wave ones. The contribution from the Pauli spin-correlation (second term in $C_{ii'}$) to the p -wave correlation function $\xi_{ii}^{(P)}$ is shown in Fig. 7 (left panel) as a function of the Fermi momentum for different kaon energies. We see that the correlation parameter decreases with the density since the core correlations hold baryons apart from each other and suppresses, thereby, the effect of the Pauli exclusion principle. The right panel of Fig. 7 presents the values of the correlation function (61) and (62) calculated for $\omega = \mu_e$ in the neutron star matter with hyperon coupling constants according to case I.

In view of their smallness, we leave the contributions from the hyperon Fermi seas to the regular part of the polarization operator $\delta\Pi_{S, \text{hyp}}^{(0)}$ without corrections for baryon-baryon correlations.

B. Correction of p -wave pole terms

We turn now to the consideration of correlation effects in the particle-hole channel.

If we approximate the free $\bar{K}N$ scattering amplitude (hatched triangle) in Eq. (58) by the hyperon-exchange diagram—the same that produces the particle-hole diagrams (26)—we can see that the account of correlations via Eq. (58) is equivalent to the replacement²

$$\text{Diagram with hatched triangle} \rightarrow \text{Diagram with fat point} \quad (65)$$

with a modified vertex (fat point) obeying equation

²The replacement (65) and (66) can be explicitly proven in the nonrelativistic limit. Working with relativistic kinematics, we apply it only to the pole part of diagram (26) written in terms of the Lindhard function (28). Thereby, we preserve the correct transition to the nonrelativistic limit.

$$\begin{array}{c}
 \text{H} \\
 \swarrow \\
 \bullet \\
 \nwarrow \\
 \text{N}^{-1}
 \end{array}
 \begin{array}{c}
 \text{---} \\
 \text{---} \\
 \text{---}
 \end{array}
 =
 \begin{array}{c}
 \text{H} \\
 \swarrow \\
 \bullet \\
 \nwarrow \\
 \text{N}^{-1}
 \end{array}
 \begin{array}{c}
 \text{---} \\
 \text{---} \\
 \text{---}
 \end{array}
 +
 \begin{array}{c}
 \text{H} \quad \text{H} \\
 \swarrow \quad \swarrow \\
 \square \\
 \nwarrow \quad \nwarrow \\
 \text{N}^{-1} \quad \text{N}^{-1}
 \end{array}
 \begin{array}{c}
 \text{---} \\
 \text{---} \\
 \text{---}
 \end{array}
 . \quad (66)$$

The particle-hole irreducible box $T_{HN'}^{\text{loc}}$ (the square) can be

$$\begin{array}{l}
 T_{\Lambda N}^{\text{loc}} = \begin{array}{c} \Lambda \\ \swarrow \quad \swarrow \\ \square \\ \nwarrow \quad \nwarrow \\ \text{N}^{-1} \quad \text{N}^{-1} \end{array} = C_0 f'_\Lambda s_{12}, \quad T_{\Sigma N}^{\text{loc}} = \begin{array}{c} \Sigma \\ \swarrow \quad \swarrow \\ \square \\ \nwarrow \quad \nwarrow \\ \text{N}^{-1} \quad \text{N}^{-1} \end{array} = C_0 g'_\Sigma s_{12} P_{\Sigma N}^{(1/2)}, \\
 T_{\Lambda \Sigma^\alpha}^{\text{loc}} = \begin{array}{c} \Lambda \quad \Sigma^\alpha \\ \swarrow \quad \swarrow \\ \square \\ \nwarrow \quad \nwarrow \\ \text{N}^{-1} \quad \text{N}^{-1} \end{array} = C_0 f'_{\Lambda \Sigma} s_{12} \tau^\alpha, \quad T_{\Sigma^* \alpha N}^{\text{loc}} = \begin{array}{c} \Sigma^* \quad \Sigma^* \\ \swarrow \quad \swarrow \\ \square \\ \nwarrow \quad \nwarrow \\ \text{N}^{-1} \quad \text{N}^{-1} \end{array} = C_0 g'_{\Sigma^*} s_{12} P_{\Sigma^* N}^{(1/2)},
 \end{array} \quad (67)$$

with $\alpha=1,2,3$. The amplitudes are normalized with $C_0=300 \text{ MeV fm}^3$ allowing for a comparison of the values for the hyperon-nucleon correlation parameters with those for the nucleon-nucleon correlations introduced in Ref. [21]. In Eq. (67), $P_{\Sigma N}^{(1/2)}=(1-\vec{t}_\Sigma \cdot \vec{\tau})/3$ is the projection operator onto the ΣN state with isospin 1/2, \vec{t}_Σ are the isospin-one matrices and $\vec{\tau}$ are the Pauli matrices of the nucleon isospin. The projector $P_{\Sigma^* N}^{(1/2)}$ is defined analogously. The spin-spin operators in the particle-hole channel are given by $s_{12}=(\vec{\sigma}_1 \vec{\sigma}_2)$ and $S_{12}=(\vec{S}_1 \vec{S}_2^\dagger)$, with \vec{S} standing for the spin operator, which couples spin- $\frac{1}{2}$ and spin- $\frac{3}{2}$ states.

The inclusion of correlations according to Eq. (66) brings the pole polarization operator (25) into the form

$$\begin{aligned}
 \Pi^{\text{pole}}(\omega, \vec{k}) &= \frac{\tilde{\Pi}_{p\Lambda}(\omega, \vec{k}) + \tilde{\Pi}_\Sigma(\omega, \vec{k}) + 2cf'_{\Lambda\Sigma} \tilde{\Pi}_{p\Lambda}(\omega, \vec{k}) \tilde{\Pi}_\Sigma(\omega, \vec{k})/3}{1 - c^2 f'_{\Lambda\Sigma} \tilde{\Pi}_{p\Lambda}(\omega, \vec{k}) \tilde{\Pi}_\Sigma(\omega, \vec{k})/3} + \Pi_{\Sigma^*}(\omega, \vec{k}), \\
 \tilde{\Pi}_{p\Lambda}(\omega, \vec{k}) &= \frac{\Pi_{p\Lambda}^{(0)}(\omega, \vec{k})}{1 - f'_\Lambda C_0 \Phi_{p\Lambda}(\omega, \vec{k})}, \quad c = C_0 / (C_{KN\Lambda} C_{KN\Sigma}), \\
 \tilde{\Pi}_\Sigma(\omega, \vec{k}) &= \frac{\Pi_{p\Sigma^0}^{(0)}(\omega, \vec{k}) + 2\Pi_{n\Sigma^-}^{(0)}(\omega, \vec{k})}{1 - g'_\Sigma C_0 [\Phi_{p\Sigma^0}(\omega, \vec{k}) + 2\Phi_{n\Sigma^-}(\omega, \vec{k})]/3}, \\
 \Pi_{\Sigma^*}(\omega, \vec{k}) &= \frac{\Pi_{p\Sigma^*0}^{(0)}(\omega, \vec{k}) + 2\Pi_{n\Sigma^*-}^{(0)}(\omega, \vec{k})}{1 - g'_{\Sigma^*} C_0 [\Phi_{p\Sigma^*0}(\omega, \vec{k}) + 2\Phi_{n\Sigma^*-}(\omega, \vec{k})]/3}. \quad (68)
 \end{aligned}$$

C. Correlation parameters

To the best of our knowledge, there is no direct experimental information about the values of the Landau-Migdal parameters for the hyperon-nucleon interactions f'_Λ , $g'_{\Sigma(\Sigma^*)}$, and $f'_{\Lambda\Sigma}$. In principle, this information could be extracted from multistrange hypernucleus data, which, however, are rather poor. In Ref. [15], the Landau-Migdal parameter f'_Λ

expressed in terms of ξ^p and kaon-nucleon-hyperon coupling constants.

Below we would like to put the discussion on a more phenomenological level. According to the arguments of the Fermi-liquid theory [56], the particle-hole irreducible box $T_{HN'}^{\text{loc}}$ has a weak dependence on incoming energies and momenta and, therefore, can be parametrized in terms of phenomenological Landau-Migdal parameters:

was estimated in line with Ref. [57], where these parameters for the nucleon-nucleon interaction were calculated within the Ericson-Ericson-Lorentz-Lorenz approach. We follow this approach below. Further corrections can be computed as in Ref. [49].

Following [57], we assume that the squared block in Eq. (67) is determined by exchanges of kaon and heavy strange vector meson K^* with mass $m_{K^*} \approx 892 \text{ MeV}$. This can be

depicted in diagrams as

$$(69)$$

In this approximation, correlation parameters are equal for the HN^{-1} and the NH^{-1} interactions. Including hyperon Fermi seas means that the pole term of the polarization operator is corrected through replacement (52) in Eq. (68). Block (69), being evaluated at the zero momentum and energy transfer, contributes to the local interaction in Eq. (67) as

$$T_{HN}^{\text{loc}} \approx C_{KNH} C_{KNH} \xi_K^{\xi(\text{P,core})}(0) + C_{K^*NH} C_{K^*NH} \xi_{K^*}^{\xi(\text{P,core})}(0),$$

$$H = \Lambda, \Sigma, \Sigma^*, \quad (70)$$

$$T_{\Lambda\Sigma}^{\text{loc}}(\omega) \approx C_{K\Lambda} C_{K\Lambda} \xi_K^{\xi(\text{P,core})}(0) + C_{K^*\Lambda} C_{K^*\Lambda} \xi_{K^*}^{\xi(\text{P,core})}(0). \quad (71)$$

For shortness, we do not write here explicitly the spin and isospin operators and note that those are exactly the same as in Eq. (67). The vector-meson coupling constants C_{K^*NH} in Eq. (70) correspond to the nonrelativistic vertex $\propto [\vec{\sigma} \times \vec{k}]$. The coupling constants can be taken from the Jülich model of the hyperon-nucleon interaction via meson exchanges [45]: $C_{K^*\Lambda} = -(1.3/m_\pi)$, $C_{K^*\Sigma} = (0.07/m_\pi)$, and $C_{K^*\Sigma^*} = (0.7/m_\pi)$. These values account for the form factors used in Ref. [45]. Particularly, the very soft form factor is responsible for a strong suppression of the $C_{K^*\Sigma}$ vertex.

Thus, the Landau-Migdal correlation parameters (67) can be cast as

$$C_0 f'_\Lambda = C_{K\Lambda}^2 [\xi_K^{\xi(\text{P,core})}(0) + R_{\Lambda\Lambda} \xi_{K^*}^{\xi(\text{P,core})}(0)],$$

$$C_0 g'_\Sigma = 3 C_{K\Sigma}^2 [\xi_K^{\xi(\text{P,core})}(0) + R_{\Sigma\Sigma} \xi_{K^*}^{\xi(\text{P,core})}(0)],$$

$$C_0 f'_{\Lambda\Sigma} = C_{K\Lambda} C_{K\Sigma} [\xi_K^{\xi(\text{P,core})}(0) + R_{\Lambda\Sigma} \xi_{K^*}^{\xi(\text{P,core})}(0)],$$

$$C_0 g'_{\Sigma^*} = 3 C_{K\Sigma^*}^2 [\xi_K^{\xi(\text{P,core})}(0) + R_{\Sigma^*\Sigma^*} \xi_{K^*}^{\xi(\text{P,core})}(0)],$$

where the first term was introduced in Eq. (63), $\xi_K^{\xi(\text{P,core})}(0) \approx 0.24$, the second one is equal to $\xi_{K^*}^{\xi(\text{P,core})}(0) = \frac{2}{3} m_0^2 / (m_0^2 + m_{K^*}^2) \approx 0.28$, cf. Ref. [57], and $R_{HH'} = C_{K^*NH} C_{K^*NH'} / (C_{KNH} C_{KNH'})$ with $R_{\Lambda\Lambda} \approx 3.7$, $R_{\Sigma\Sigma} \approx 0.04$, $R_{\Lambda\Sigma} \approx 0.39$, and $R_{\Sigma^*\Sigma^*} \approx 0.69$. The additional factor 2 in $\xi_{K^*}^{\xi(\text{P,core})}$ compared to $\xi_K^{\xi(\text{P,core})}$ originates from the reduction $[\vec{\sigma}_2 \times \vec{k}][\vec{\sigma}_1 \times \vec{k}] \rightarrow s_{12}$. Finally, we estimate the following values for the correlation parameters of Eq. (67) as

$$f'_\Lambda \approx 0.9, \quad g'_\Sigma \approx 0.1, \quad f'_{\Lambda\Sigma} \approx -0.1, \quad g'_{\Sigma^*} \approx 1.2. \quad (72)$$

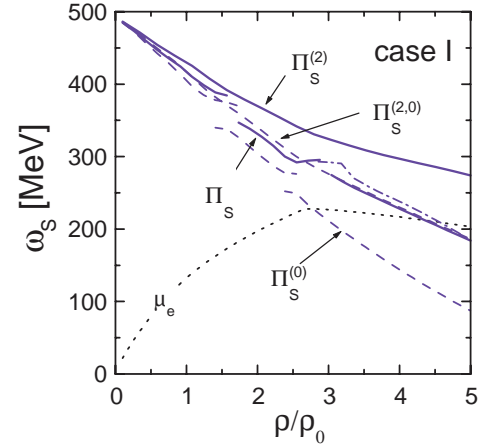


FIG. 8. Solid lines present the energy of the lowest branch of the dispersion equation at $\vec{k}=0$ calculated with the polarization operators $\Pi_S^{(2)}$ and Π_S including effects of baryon-baryon correlations. Dashed-dotted continuations of solid curves demonstrate effect of the filling of the hyperon Fermi seas on the s -wave polarization operator. Correlation parameters are taken according to Fig. 7 (right panel), (61) and (72). Dashed lines show solutions $\Pi_S^{(2,0)}$ and $\Pi_S^{(0)}$ without correlation effects, as in Fig. 5, panel (b). The dotted line depicts the electron chemical potential.

Compared to Ref. [15], we obtained a smaller value of the parameter $C_0 f'_\Lambda \approx 0.6/m_\pi^2$, since we included here the form factors mentioned above.³

D. Energy of the lowest branch of the dispersion relation at $\vec{k}=0$

Figure 8 illustrates how strongly the kaon spectrum changes after including the short-range correlations. We show the lowest branch of the kaon spectrum at $\vec{k}=0$. This is calculated for the polarization operator $\Pi_S^{(2)}$ constructed from $\Pi_S^{(2,0)}$ according to Eq. (59) and for the polarization operator $\Pi_S(\omega) = \Pi_S^{(2)}(\omega) + \Pi^{\text{pole}}(\omega, 0)$, where $\Pi^{\text{pole}}(\omega, 0)$ follows from Eq. (68) with parameters (72). The hyperon couplings are chosen according to case I.

At $\rho > \rho_{c,H}$, we have to include correlations in the term $\delta\Pi_{S,\text{hyp}}^{(0)}$ in Eq. (56). The pole term $\delta\Pi_{\text{hyp}}^{(\text{pole},0)}(\omega, 0)$ is included in Eq. (68) with the help of replacement (52). The other terms $\delta\Pi_{S,\text{hyp}}^{(\chi\text{PT},0)}(\omega)$ and $\delta\Pi_{S,h}^{(0)}$ can be corrected in the same manner as the $\Pi_S^{(0)}$ term. However, these terms are rather small as it is demonstrated by Fig. 6. Therefore, we omit correlations in them.

From Fig. 8, we see that baryon-baryon correlations suppress the s -wave part of the polarization operator, in agreement with the statements [53,54]. It results in an increase of the critical density of the s -wave condensation from $2.7\rho_0$ to $4.3\rho_0$ for case I, chosen as an illustration.

³Note that different normalizations of Landau-Migdal parameters are used here and in Ref. [15].

VIII. K^- CONDENSATION IN NEUTRON STARS

In Secs. IV–VII, we have constructed the K^- polarization operator. Now we use it to study a possible instability of the system with respect to a phase transition into a state with K^- condensate.

First, we investigate the solutions of the K^- dispersion relation

$$\omega^2 - \vec{k}^2 - m_K^2 - \text{Re}\Pi^{\text{tot}}(\omega, \vec{k}) = 0, \quad (73)$$

where the complete polarization operator is given by

$$\begin{aligned} \Pi^{\text{tot}}(\omega, \vec{k}) = & \Pi_S(\omega) + \Pi_P^{\text{reg}}(\omega, \vec{k}) + \Pi_P^{\text{pole}}(\omega, \vec{k}) + \delta\Pi_{\text{hyp}}^{(\chi\text{PT},0)}(\omega) \\ & + \delta\Pi_{\text{hyp}}^{\text{reg},0}(\omega). \end{aligned} \quad (74)$$

It contains the s -wave part, the regular p -wave, and the pole parts of the polarization operator given by Eqs. (59), (60), and (68), respectively, and the terms determined by the hyperon populations (54) and (55). The correlation parameters are taken according to Eqs. (61), (62), and (72).

There are two different possibilities: K^- condensation may occur in neutron star matter via a second-order phase transition or a first-order phase transition. The dynamics of these phase transitions is quite different. Both possibilities might be realized at different physical conditions related to different stages of a neutron star evolution.

In case of a second-order phase transition, at the moment, when the density in the neutron star center achieves the critical density ρ_c^{II} , reactions (1) become operative. At this transition, the isospin composition and the density of the system change smoothly. During the time $\tau \propto \tau_{\text{react}} \sqrt{\rho_c^{\text{II}} / \sqrt{\rho - \rho_c^{\text{II}}}}$, where τ_{react} is the typical time of the weak processes (1), the system creates an energetically favorable condensate state. The condensate appears within the region where $\rho > \rho_c^{\text{II}}$. If this happens during a supernova explosion, the typical size of the condensate region might become of the order of the neutron star radius. Due to energy conservation, the gained energy must be released in such a transition. When the condensate region is heated up to the temperatures $T \geq T_{\text{opac}} \sim (1-2)\text{-MeV}$ neutrinos are trapped. At this stage, the cooling time is determined by the neutrino heat transport from the condensate interior to the star surface [21]. When the star cools down to temperatures $T < T_{\text{opac}}$, the neutron star becomes transparent for neutrinos, and these can be directly radiated away. A part of the energy is also radiated by photons from the star surface. In binary long-living systems, the critical density in the neutron star center can be achieved by accretion. Then, the transition is characterized by the typical accretion time.

In case of a first-order phase transition, the final state might significantly differ from the initial one in its isospin composition and its density. Thus, this new state cannot be prepared in microscopic processes. Small-size droplets of the new phase are not energetically favorable due to a positive surface energy. When the density in the star center exceeds the value $\rho_c^{\text{I}} < \rho_c^{\text{II}}$, the system arrives at a metastable state. In this state, a droplet with the density $\rho_c^{\text{fin}} > \rho_c^{\text{I}}$ and a suffi-

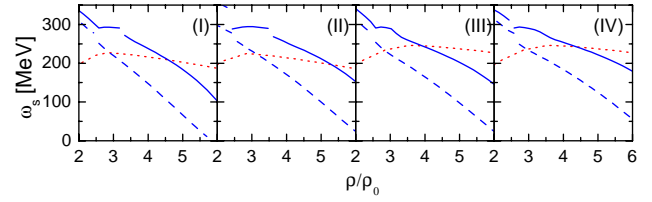


FIG. 9. Solid lines are the energy of the lowest K^- branch of the dispersion relation (73) for $\vec{k}=0$. Dotted lines show electron chemical potentials. Dashed lines are calculated without baryon-baryon correlations. Different panels correspond to the interactions given by cases I–IV.

ciently large (overcritical) size, created by fluctuations, will continue growing. At zero temperature, the probability for the creation of such a droplet via quantum fluctuations is very small, but it increases greatly with the temperature [21]. Thus, a first-order phase transition is most likely at an initial stage of a neutron star formation or cooling when the temperature is sufficiently large. If the density in the center of a star exceeds the value ρ_c^{II} , a second-order phase transition occurs. In long-living binary stellar systems, where the neutron star slowly accretes the mass from a star companion and the temperature is already very small, a second-order phase transition is a more probable one (depending on the accretion rate).

A. Second-order phase transition to the s -wave condensate state

Let us first analyze the possibility of the s -wave K^- condensation. In Fig. 9, we summarize the results of Secs. V C, VI C, and VII D, showing the energy of the lowest K^- branch of the kaon dispersion relation (73) for $\vec{k}=0$ together with the electron chemical potential. For the given parameter choice, the crossing points of the lines indicate the critical density of the s -wave condensation via a second-order phase transition.

We see that for all models the neutron star matter is unstable with respect to the reactions in Eq. (1) at densities $(3-5.2)\rho_0$. The critical density depends on the choice of the correlation parameters and the parameters of the hyperon-nucleon interactions. As long as correlations are not included, we support the conjecture of previous works on the possibility of the s -wave condensation at $\rho_{c,S}^{(\text{II})} \sim 3\rho_0$. However, the baryon-baryon correlations shift the condensation critical density to values larger than those ones discussed in Refs. [5,7–12].

B. Second-order phase transition to the p -wave condensate state

In this section, we study a principal possibility for the p -wave K^- condensation in neutron star matter via a second-order phase transition. We investigate whether the p -wave condensation can occur before the s -wave condensation and to what extent this depends on the parameters of hyperon-nucleon interactions and correlations.

Let us first assume that the s -wave K^- condensation is indeed possible at some critical density $\rho_{c,S}$. The lowest en-

ergy branch of the K^- spectrum at small momenta is given by

$$\omega \approx \omega_S + \alpha(\omega_S) Z_S(\omega_S) \vec{k}^2, \quad (75)$$

where ω_S is, as before, $\omega(\vec{k}=0)$ for the lowest energy branch of the dispersion law given by the solution of the equation $\omega_S^2 = m_K^2 + \text{Re}\Pi_S(\omega_S, \vec{k}=0)$, and

$$Z_S^{-1}(\omega) = \left(2\omega_S - \frac{\partial \text{Re}\Pi_S(\omega, \vec{k})}{\partial \omega} \Big|_{\vec{k}=0} \right) > 0,$$

$$\alpha(\omega) = 1 + \frac{\partial \text{Re}\Pi_P(\omega, \vec{k})}{\partial \vec{k}^2} \Big|_{\vec{k}=0}.$$

If at $\rho_{c,S}$, we have $\alpha(\omega_S) < 0$, then instead of the s -wave condensation we have the p -wave condensation at a somewhat smaller density. The aim of this section is to find the value $\alpha(\omega_S)$ in Eq. (75) at the critical point of the s -wave condensation, i.e., when $\omega_S = \mu_e$.

Using the p -wave kaon polarization operator determined in Sec. V, we write

$$\alpha(\omega) = 1 + \alpha_{\text{pole}}(\omega) + \alpha_{\text{reg}}(\omega). \quad (76)$$

Without baryon-baryon correlations, the contribution of the pole part is

$$\alpha_{\text{pole}}^{(0)} = \frac{\partial}{\partial \vec{k}^2} \text{Re}\Pi^{(\text{pole},0)}(\omega, \vec{k}) \Big|_{\vec{k}=0} = \alpha_{\Lambda p}^{(0)} + \alpha_{\Sigma}^{(0)} + \alpha_{\Sigma^*}^{(0)}, \quad (77)$$

with $\alpha_{\Sigma}^{(0)} = \alpha_{\Sigma_0 p}^{(0)} + 2\alpha_{\Sigma^- n}^{(0)}$ and $\alpha_{\Sigma^*}^{(0)} = \alpha_{p\Sigma^* 0}^{(0)} + 2\alpha_{n\Sigma^* -}^{(0)}$. From Eqs. (37) and (38), we have

$$\alpha_{iH}^{(0)}(\omega) = C_{KNH}^2 [\eta_{NH}^2 \phi_{iH}^P(\omega) + \eta_{HN}^2 \phi_{Hi}^P(-\omega)],$$

$$\alpha_{i\Sigma^*}^{(0)}(\omega) = C_{KN\Sigma^*}^2 \eta_{N\Sigma^*}^2 \Phi_{i\Sigma^*}(\omega, 0), \quad H = \{\Lambda, \Sigma\}.$$

The term $\eta_{HN}^2 \phi_{iN}^P(-\omega)$ accounts for the contribution of the hyperon Fermi sea. Once the baryon-baryon correlations are included in the pole part of the polarization operator according to Eq. (68), $\alpha_{\text{pole}}^{(0)}$ is to be replaced by

$$\alpha_{\text{pole}}(\omega) = \frac{\partial}{\partial \vec{k}^2} \text{Re}\Pi^{\text{pole}}(\omega, \vec{k}) \Big|_{\vec{k}=0}.$$

The regular part follows from Eq. (39), $\alpha_{\text{reg}}^{(0)}(\omega) = b_p(\omega) \rho_p / \rho_0 + b_n(\omega) \rho_n / \rho_0$, with the coefficients defined in Eq. (40). The suppression of the regular part α_{reg} due to the baryon-baryon correlations can be taken into account, according to Eq. (60)

$$\alpha_{\text{reg}}(\omega) = \frac{\tilde{b}_p(\omega) + \tilde{b}_n(\omega) + 2\tilde{b}_p(\omega)\tilde{b}_n(\omega)\xi_{np}^{(P)}(\omega)}{1 - \tilde{b}_p(\omega)\tilde{b}_n(\omega)(\xi_{np}^{(P)})^2(\omega)},$$

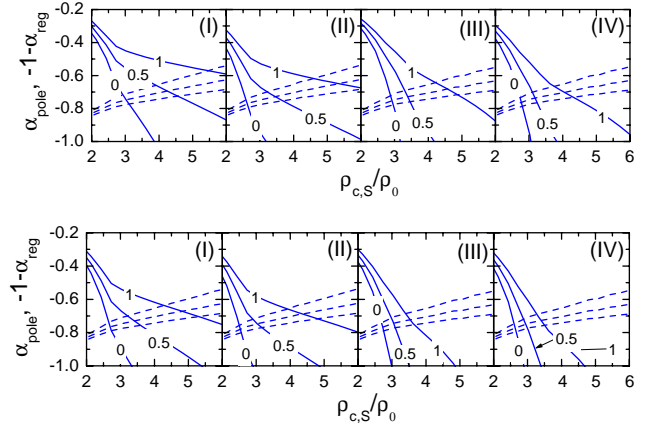


FIG. 10. $\alpha_{\text{pole}}(\mu_e)$, $\omega_S = \mu_e$, (solid lines), and $-1 - \alpha_{\text{reg}}$ (dashed lines) vs critical density of the s -wave K^- condensation for various correlation parameter choices. Labels show values of $f_{\Lambda}^{\prime} = g_{\Sigma}^{\prime}$. Solid lines are drawn for $f_{\Lambda}^{\prime} = 0$, and $f_{\Lambda}^{\prime} = g_{\Sigma}^{\prime} = 0, 0.5, 1$. Dashed lines are for three choices of the correlation parameters used in calculation of α_{reg} , $\xi_{nn} = \xi_{pp} = \xi_{np} = 0, 0.5, 1$ (from the upper line to the lower one). Cases I–IV correspond to those in Fig. 1. In the upper plot, Σ^* is taken with $g_{\Sigma^*}^{\prime} = g_{\Sigma}$, $V_{\Sigma^*} = V_{\Sigma}$, and $g_{\sigma\Sigma^*} = g_{\sigma\Sigma}$. In the lower plot, $V_{\Sigma^*} = 0$ and $g_{\sigma\Sigma^*} = 0$. Hyperon populations are included in the mean fields but not in the polarization operator.

$$\tilde{b}_p(\omega) = \frac{b_p(\omega) \rho_p / \rho_0}{1 - b_p(\omega) \rho_p \xi_{pp}^{(P)}(\omega) / \rho_0},$$

$$\tilde{b}_n(\omega) = \frac{b_n(\omega) \rho_n / \rho_0}{1 - b_n(\omega) \rho_n \xi_{nn}^{(P)}(\omega) / \rho_0}. \quad (78)$$

Although the $\xi_{ii}^{(P)}(\omega)$ functions can be evaluated as in Eq. (62), we will treat them here as free energy-independent parameters ξ_{ii}' in order to investigate the sensitivity of the results to their variation.

In Figs. 10 and 11 we show the values of $\alpha_{\text{pole}}(\mu_e)$ (solid lines) and $-1 - \alpha_{\text{reg}}$ (dashed lines), calculated as a function of $\rho_{c,S}$ for various baryon-baryon correlation parameters and hyperon couplings. The Σ hyperon contribution is proved to be very small. The major contribution to the strength is due to Λp^{-1} and $\Sigma^* n^{-1}$ loops. The hyperon Fermi seas are not incorporated for the moment (we drop terms $\propto \Phi_{Hi}$ in Π^{pole}). Inclusion of Σ^* into the mean-field model (2) is quite uncertain due to the absence of any empirical constraint on the coupling constants. We consider two different cases: In the upper plot in Fig. 10, we assume that Σ^* couples to the mean field with the same strength as the Σ hyperon ($V_{\Sigma^*} = V_{\Sigma}$, $g_{\sigma\Sigma^*} = g_{\sigma\Sigma}$); in the lower plot in Fig. 10, we detach Σ^* from the mean-field potentials ($V_{\Sigma^*} = 0$, $g_{\sigma\Sigma^*} = 0$).

At the crossing point of the solid line with the corresponding dashed line, we have $\alpha_{\text{pole}} = -1 - \alpha_{\text{reg}}$ and therefore, $\alpha = 0$. This means that the given density is the critical density for both the s - and the p -wave condensations. For values of $\rho_{c,S}$, for which the solid line is below the corresponding dashed line $\alpha_{\text{pole}} < -1 - \alpha_{\text{reg}}$. This means that $\alpha < 0$ and for

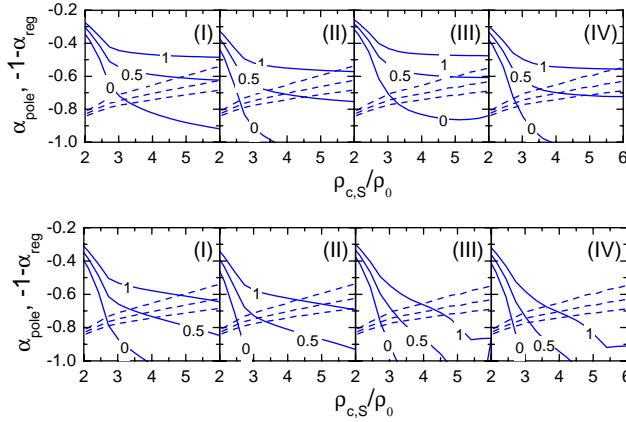


FIG. 11. Same as in Fig. 10, but with account for the hyperon population in the polarization operator.

such a parameter set K^- condensation occurs in the p -wave state at a density somewhat smaller than that assumed for the s -wave condensation.

Contributions from the hyperon Fermi seas are included in Fig. 11. Comparing Figs. 10 and 11, we see that the hyperon population affects noticeably the p -wave attraction. Figures 10 and 11 also show that the Σ^* hyperons contribute significantly to the K^- polarization operator, increasing the attraction in the p wave. The most favorable case for the p -wave condensation is realized when Σ^* is detached from the mean-field potentials.

In Fig. 12, we show the results for the values of the correlation parameters evaluated in Sec. VII. For Σ^* hyperons detached from the mean-field potentials our model predicts a preference for the p -wave condensation. The p -wave condensation is preferred at $\rho_{c,s} \leq 3.5\rho_0$ for the cases II and IV, and at $\rho_{c,s} \approx 4\rho_0$ and $\rho_{c,s} \approx 4.5\rho_0$ for cases III and I, provided the s -wave softening of the spectrum is also rather high. For Σ^* coupled with the same strength as Σ , s -wave condensation might be preferable to the p -wave condensation.

C. First-Order phase transition to the K^- condensate state

In the previous two sections, we have studied the possibility of K^- condensation assuming that this occurs via a second-order phase transition. Here, we investigate the properties of K^- excitations in baryonic matter of different particle compositions, in order to understand whether an abrupt (of a first order) phase transition into a state with new particle composition and new baryon density can be energetically favorable.

We consider (i) nucleon-hyperon matter (NHM) with a composition which we have discussed above (see Fig. 1); (ii) neutron-proton matter (NPM) consisting only of protons and neutrons in β equilibrium; (iii) isospin-symmetrical nuclear matter (ISM) consisting of protons and neutrons with $\rho_p = \rho_n$ and leptons that compensate for the electric charge of the protons; and (iv) proton-enriched matter (PEM) consisting of protons and neutrons with concentration $Y_p = \rho_p / \rho = 0.7$ and charge compensated by the leptons. Thus, in cases (ii)–(iv), we switch off the hyperons in our mean-field model

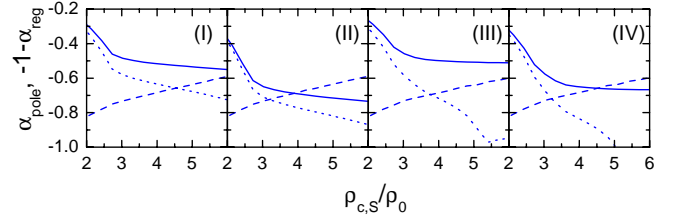


FIG. 12. Values α_{pole} (solid lines) and $-1 - \alpha_{\text{reg}}$ (dashed lines), $\omega_s = \mu_e$, calculated for the correlation parameters (72). Solid lines are calculated with Σ^* hyperons coupled to the mean field as strong as Σ hyperons. Dotted lines are with Σ^* detached from the mean-field potentials. Cases I–IV correspond to various sets of hyperon coupling constants. Contributions from the hyperon populations are included.

(2) and in cases (iii) and (iv) we also freeze the value of the proton concentration. For each case, we calculate the total energy of the system with and without K^- condensation.

In Fig. 13, we show the energy of the lowest K^- branch for the dispersion equation (73), $\omega^{\min}(\vec{k}_m, Y_p, \rho)$ minimized with respect to the momentum as a function of baryon density for different proton concentrations. We see that the more protons exist in the matter, the smaller is the value of the density at which the kaon energy $\omega^{\min}(\vec{k}_m, Y_p, \rho)$ meets the electron chemical potential. Therefore, if the energy gain due to the condensation is large enough to compensate an energy loss due to fermion kinetic energies, the system undergoes a first-order phase transition from the NHM state to the state with a proton-enriched composition and a different density.

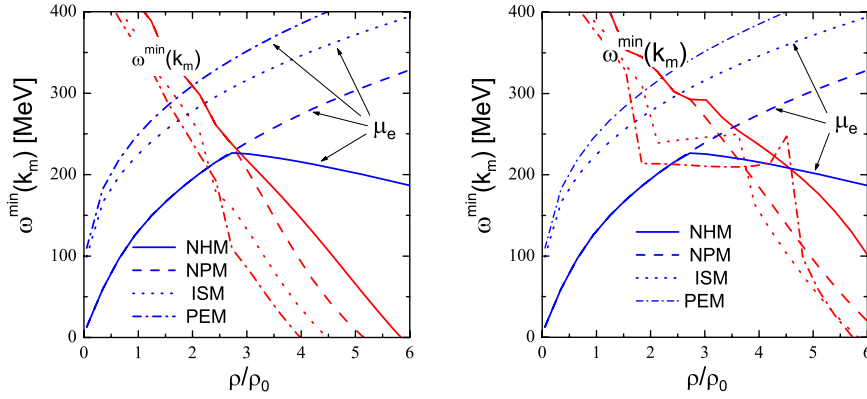
Let us first compare the energies of NHM, NPM, ISM, and PEM taking into account the possibility for the K^- condensation in each case. For densities $\omega^{\min}(\vec{k}_m, Y_p, \rho) > \mu_e$, there is no condensation and the energy density of the system is given by Eq. (4). When $\omega^{\min}(\vec{k}_m, Y_p, \rho) < \mu_e$, the K^- excitations appear, replacing partially the leptons. These excitations occupy a single state with the lowest energy and form a K^- condensate. The electron chemical potential is fixed now as $\mu_e = \omega^{\min}(\vec{k}_m, Y_p, \rho)$. The energy density of the system with the K^- condensate reads

$$E_{\text{tot}}^{(K)} = E_{\text{mes}} + \sum_B E_B^{\text{kin}} + \sum_{l=\mu_e} E_l(\omega^{\min}(\vec{k}_m, Y_p, \rho)) + E_{\text{cond}}^{(K)}, \quad (79)$$

where $E_{\text{cond}}^{(K)}$ is the energy density of the condensate field related to the mean-field Lagrangian

$$\mathcal{L}_K = [\omega^2 - m_K^2 - \vec{k}^2 - \Pi(\omega, \vec{k})] |\phi_{\vec{k}}|^2. \quad (80)$$

The $\phi_{\vec{k}}$ is the K^- condensate mean field with the wave vector \vec{k} . This field component should be found from the minimization of an appropriate thermodynamical potential. For simplicity, we neglect higher-order terms, such as $\propto |\phi_{\vec{k}}|^4$, which represent an effective kaon-kaon interaction in dense baryonic matter. The effective kaon-kaon interaction depends on the structure of the mean field. In the absence of a nonlinear effective kaon-kaon interaction, the



condensate field is of the running plane-wave type, $\phi_{\vec{k}} = \exp[-i\omega^{\min}(\vec{k}_m, Y_p, \rho)t + i\vec{k}_m \vec{r}]$. The dispersion relation (73) is fulfilled for $\vec{k} = \vec{k}_m$ and $\omega = \omega^{\min}(\vec{k}_m, Y_p, \rho)$, and the density of the charged kaon condensate ρ_K is fixed by the electroneutrality condition

$$\rho_K = \sum_B q_B \rho_B - \rho_e - \rho_{\mu^-},$$

and thus, the energy density of the kaon condensate equals

$$E_{\text{cond}}^{(K)} = \omega^{\min}(\vec{k}_m, Y_p, \rho) \left(\sum_B q_B \rho_B - \rho_e - \rho_{\mu^-} \right).$$

In Fig. 14, we show the energy per baryon in various baryonic systems, NHM, NPM, ISM, and PEM ($Y_p \approx 0.7$), with and without the kaon condensate (dashed and solid lines, respectively). We see that for a density $\rho_c \approx 3\rho_0$ without baryon-baryon correlations and $\approx 4\rho_0$ with correlations, the condensate state in ISM becomes energetically favorable compared to NHM. The transition to the new, more symmetrical isospin configuration increases the Fermi energies of the leptons (the latter ones are needed to compensate a larger charge of protons), but reduces the symmetry energy of nuclear matter and also the total Fermi energy of nucleons. Without a K^- condensate, the energy loss is larger than the gain and the system chooses NHM with the composition shown in Fig. 1 (in Fig. 13, the ISM lines lie above the NPM lines). With the K^- condensation, the energy of the system decreases significantly since leptons are replaced by kaons. The latter energy gain is large enough to support the

preference of ISM. From Fig. 14, we see that PEM ($Y_p \approx 0.7$) has a larger energy than ISM. As it is also seen from Fig. 14, the resulting isospin composition can be only slightly above $Y_p = 1/2$. In the following, we neglect this small difference and consider ISM as the final configuration.

In Fig. 15, we plot the lowest branch of the K^- excitation spectrum $\omega_{\min}(\vec{k})$ in the ISM at various densities. On the left panel, baryon-baryon correlations are switched off and on right panel, switched on. We see that for densities $\geq (2.5-3.5)\rho_0$, the spectra have minima (dots in Fig. 15) at finite values of the kaon momentum $\vec{k}_m \neq 0$. This signals that the transition from NHM to a dense ISM would occur as a first-order phase transition into the state with the p -wave kaon condensate. The calculations shown in Figs. 13–15 are done for $g'_{\Sigma^*} = g_{\Sigma}$, $V_{\Sigma^*} = V_{\Sigma}$, and $g_{\sigma\Sigma^*} = g_{\sigma\Sigma}$. The results obtained with the Σ^* hyperons detached from the mean-field potentials are checked to be of minimal difference.

Assuming that the surface tension is large enough, the initial and final state densities can be determined by the double-tangent Maxwell construction [58,59]. In Fig. 16, we show such a construction between NHM and ISM states. We see that the critical density for the beginning of a first-order phase transition is equal to $\rho_c^I \approx 1.4\rho_0$ without correlations and $\approx 2.1\rho_0$ with correlations. The critical densities of the final state are $\rho_{\text{fin}}^I \approx 5\rho_0$ and $\approx 6\rho_0$, respectively.

If the surface tension is smaller than some critical value then the phase transition results in the mixed phase [60,58,61,59]. In such a case, the local charge-neutrality condition is to be replaced by the global charge-neutrality con-

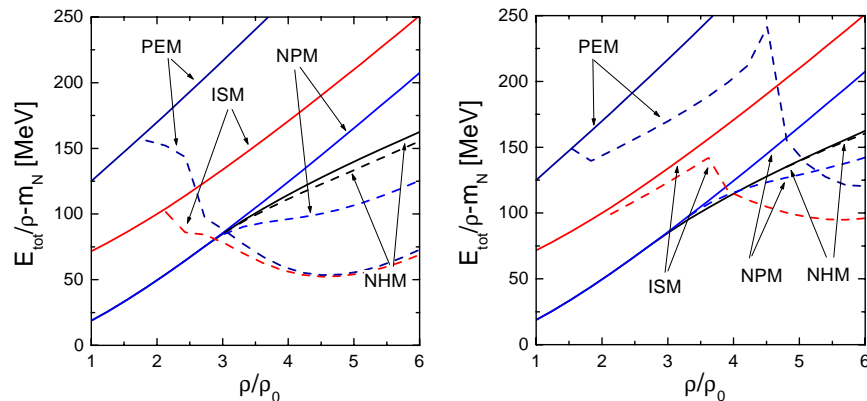


FIG. 14. Total energy per baryon of matter with different particle compositions: without (solid lines) and with (dashed lines) the K^- condensate. Abbreviations are the same as in Fig. 13. The curves in the right and the left panels are drawn with and without inclusion of correlations, respectively. In the NHM case, the parameters are the same as in Fig. 13.

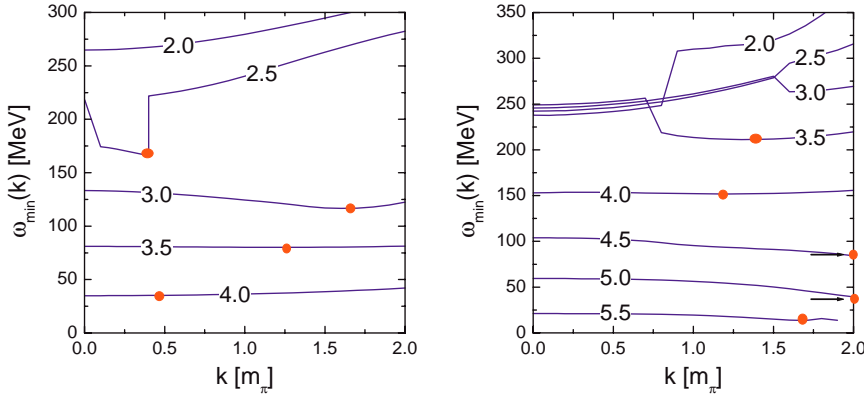


FIG. 15. The energy of the lowest branch of the dispersion equation (73) as function of the momentum for the ISM at various densities (labels are densities in ρ_0). The polarization operator is taken according to Eq. (74). Calculations without and with baryon-baryon correlations are shown on left and right panels, respectively. Full circles mark the position of the minimum.

dition. The critical density for the appearance of kaon condensate droplets within a mixed phase is still smaller than the value given by Maxwell construction. The presence of the mixed phase may have interesting observable consequences (see Ref. [62], and references therein).

Thus, relying on the analysis above, we argue that the critical density of a first-order phase transition can be even smaller than $2\rho_0$, and that such transition occurs into the p -wave condensate state.

IX. CONCLUSION

In this work, we constructed the K^- polarization operator in dense baryonic matter of arbitrary isotopic composition, including both the s - and p -wave K^- -baryon interactions. We used a relativistic mean-field model to describe the baryon properties. The polarization operator was applied then to study the s - and p -wave K^- condensations in neutron star interiors. The results are presented for two different models of the equation of state, cf. Sec. II and Appendix A. Finite temperature effects can easily be incorporated in our general scheme.

To describe the kaon-nucleon interaction, we used the kaon-nucleon scattering amplitude obtained as a solution of the coupled-channel Bethe-Salpeter equation with an interaction kernel derived from a relativistic chiral SU(3) Lagrangian with the large N_c constraints of QCD [16]. The Λp^{-1} , ΣN^{-1} , $\Sigma^* N^{-1}$ particle-hole contributions were taken into account in the polarization operator. Effects of the filling of

the hyperon $H=(\Lambda, \Sigma, \Xi)$ Fermi seas at densities above the hyperonization point $\rho > \rho_{c,H} \approx (2.5-3)\rho_0$ are analyzed.

In Fig. 5, we compared the regular s -wave part of the polarization operator with the simplified form widely used in the literature. The kaon-nucleon Σ term extracted from this comparison ($\Sigma \approx 150$ MeV) was found to be two to three times smaller than what allows for the s -wave K^- condensation in ordinary neutron star matter composed mostly of neutrons. However, we found a sizable attractive support from the hyperon exchange terms of the p -wave scattering amplitude contributing to the s -wave part of the polarization operator. Inclusion of these terms, which were omitted in previous works, makes a second-order phase transition to the s -wave K^- condensate state possible at densities $\approx 3\rho_0$ when the correlation effects are not included.

We evaluated baryon-baryon short-range correlation parameters and corrected all the s - and p -wave terms of the polarization operator, accordingly. The correlations increased the critical point of a second-order phase transition to the s -wave K^- condensate state to densities $\approx (4-5)\rho_0$, (see Fig. 9). We estimated (see Appendix C) the effects of the kaon fluctuations. Their contributions are small at low kaon energies, and as first approximation at zero temperature, they can be neglected.

Our next observation (see Appendix C) was that at $\vec{k} = 0$, the imaginary part of the pole term of the polarization operator is finite only in a rather narrow interval of kaon energies. If the electron chemical potential crosses the K^- branch within this energy interval, the s -wave condensation

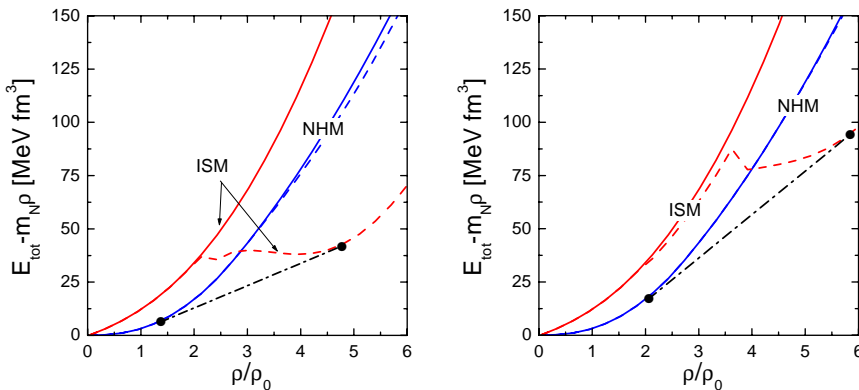


FIG. 16. Energy densities of NHM and ISM with and without the K^- condensate shown by dashed and solid lines, respectively. For NHM, the forces of case I are used. Calculations with and without baryon-baryon correlations are shown in left and right panel, respectively. The dash-dotted lines represent double-tangent Maxwell constructions between two phases.

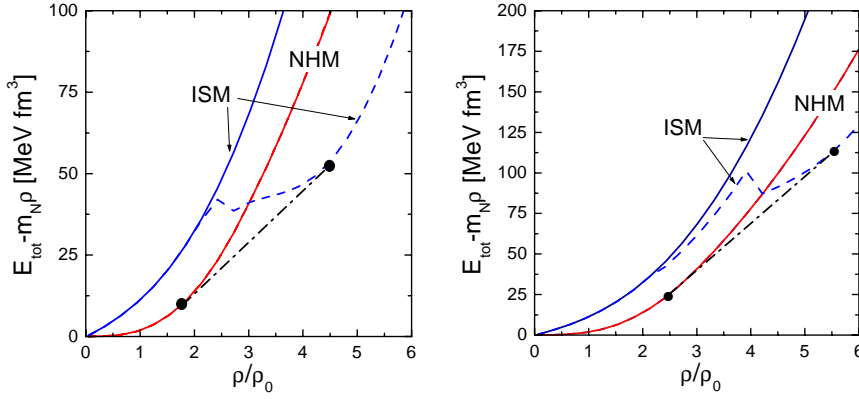


FIG. 19. Same as in Fig. 16 but for parameters (A1).

will not occur. However, this possibility is not realized for the parameter choice used in our model.

Further, we have investigated the possibility of a second-order phase transition to the p -wave K^- condensate state. We showed that in the vicinity of the critical point of the s -wave K^- condensation the p -wave part of the polarization operator, induced mainly by Λ -proton holes and Σ^* -nucleon holes, and some regular terms, is large and attractive. This may change the sign of the momentum derivative of the energy at the lowest K^- spectrum branch at the origin. If this occurred, it would mean that there is a p -wave condensate instead of an s -wave one appearing at somewhat smaller density. This statement, although rather model dependent, holds for a wide range of varying parameters. The results depend essentially on the Σ^* hyperon coupling to the mean-field potentials. In the most favorable case, when Σ^* is detached from the mean-field potentials, the second-order phase transition to the p -wave condensate state may occur already at $\rho \sim 3\rho_0$ (with correlations included), cf. Fig. 12. This result is also sensitive to the details of the equation of state and to the parametrization of the hyperon-nucleon interaction. For an equation of state with the parameters from Eq. (A1), the critical density is increased with respect to the one calculated with the parameters defined in Eq. (5).

We have also discussed the possibility of a first-order phase transition to a K^- condensate state. We have found that in the presence of a K^- condensation, the isospin-symmetrical neutron-proton matter is energetically favorable than the standard nucleon-hyperon-lepton matter for densities $\geq (3-4)\rho_0$ (depending on the values of parameters of baryon-baryon correlations). This yields a possibility for a first-order phase transition. At such a transition, hyperons are replaced by nucleons and electrons are replaced by the condensate K^- mesons. In dense, isospin-symmetrical nuclear matter K^- excitations are condensed in the p -wave state. With the help of Maxwell construction, we found that the critical density at the beginning of the phase transition is about $2\rho_0$ with the baryon-baryon correlations included, cf. Figs. 16 and 19. The final state density is about $(5-6)\rho_0$. Occurrence of such a strong first-order phase transition may have interesting observable consequences: blowing-off a part of the exterior of the neutron star, strong neutrino pulls, gravitational waves, strong pulsar glitches, etc. These effects have been previously discussed in relation to a first-order phase transition to the pion condensate state [21]. Here, we

may expect a stronger energy release compared to the pion condensate phase transition since the typical energy scale is larger, $m_K \gg m_\pi$.

Our derivations can be helpful not only for the description of neutron star interiors, but also for discussion of kaonic effects in other nuclear systems, such as atomic nuclei and in the systems formed in heavy-ion collisions. Therefore, of particular interest is the further more detailed analysis of the p -wave effects on K^- spectra in nucleus-nucleus collisions, also motivated by present SIS and SPS experiments and the future SIS200 program at GSI.

ACKNOWLEDGMENTS

The authors acknowledge J. Knoll, T. Kunihiro, M. F. M. Lutz, A. Mocsy, T. Muto, G. Ripka, T. Tatsumi, and W. Weise for stimulating discussions. D.N.V. highly appreciates hospitality and support of GSI Darmstadt. This work was supported in part by DFG (Project Nos. 436 Rus 113/558/0 and 436 Rus 113/558/0-2) and by RFBR Grant No. NNIO-00-02-04012.

APPENDIX A: VARIATION OF THE PARAMETERS OF THE BARYON INTERACTION

In this section, we investigate the sensitivity of the results of Sec. VIII to the particular choice of the EoS. For comparison, we adjust the parameters of the mean-field model to reproduce the EoS from Ref. [63], which is a good fit to the optimal EoS of the Urbana-Argonne group [26] up to four times the nuclear saturation density and smoothly incorporates the causality limit at higher densities. The corresponding coupling constants of Lagrangian (2) are

$$\frac{g_{\omega N}^2 m_N^2}{m_\omega^2} = 91.25, \quad \frac{g_{\sigma N}^2 m_N^2}{m_\sigma^2} = 195.6, \quad \frac{g_{\rho N}^2 m_N^2}{m_\rho^2} = 77.50,$$

$$b = 0.08675, \quad c = 0.08060. \quad (\text{A1})$$

These correspond to the following bulk parameters of nuclear matter at saturation: $\rho_0 = 0.16 \text{ fm}^{-3}$, binding energy $E_{\text{bind}} = -15.8 \text{ MeV}$, compression modulus $K = 250 \text{ MeV}$, symmetry energy $a_{\text{sym}} = 28 \text{ MeV}$, and the effective nucleon mass $m_N^*(\rho_0) = 0.8m_N$.

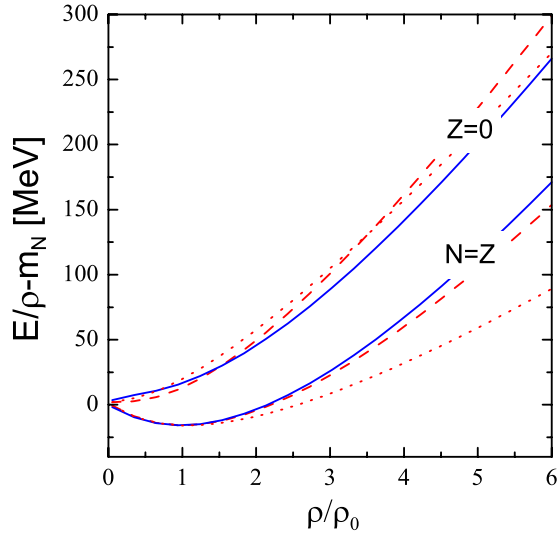


FIG. 17. The EoS for ISM ($N=Z$) and neutron matter ($Z=0$) calculated with the parameter set (5) (dotted lines) and (A1) (dashed lines). Solid lines show the EoS from Ref. [63].

In Fig. 17, we show energies for the nucleon isospin-symmetrical matter and the pure neutron matter for two choices of the mean-field EoS, model (5), simulating a softer EoS and (A1) simulating a stiffer Urbana-Argonne EoS. Even though parameters (5) and (A1) are rather different, energies and other thermodynamic characteristics of the neutron star matter are rather close to each other for both parameter choices in the absence of a K^- condensate. For the ISM case, the EoS with parameters (A1) is significantly stiffer than the one calculated with parameters (5) at $\rho \gtrsim 3\rho_0$.

In Fig. 18, we show concentrations of the baryon species in neutron star matter corresponding to the EoS given by choice (A1) for the four choices of the hyperon-nucleon interaction (cases I–IV) which we have used throughout this paper. We see that the critical density of the hyperonization is $\approx 3\rho_0$ for all choices. The general trends are the same as the ones in Fig. 1. The most essential difference is that the proton concentrations in Fig. 18 are smaller than those in Fig. 1. This should have consequences for the neutrino cooling of neutron stars. Indeed, when the proton concentration exceeds 11%–14% an efficient cooling mechanism becomes operative via the direct Urca processes $p \rightarrow n + e + \bar{\nu}$. This difference might be used, in principle, to select the more appropriate EoS.

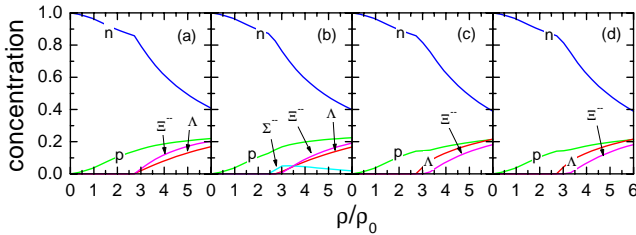


FIG. 18. Concentration of baryon species in neutron star matter for EoS (A1). Four panels correspond to four choices of the hyperon-nucleon interaction parameters specified in text.

The calculations show that a second-order phase transition to the s -wave K^- condensate state occurs at densities $(3.5\text{--}6)\rho_0$, depending on the choice of the parameters. A second-order phase transition to the p -wave state may occur in model (A1) for $\rho \gtrsim (4.5\text{--}5.5)\rho_0$ in cases II–IV, and it does not occur for case I up to $6\rho_0$.

In Fig. 19, we show the double-tangent construction for the EoS with the parameters of Eq. (A1). The first-order phase transition starts at the density $\rho_c^1 \approx 2.5\rho_0$ (with correlations included). This value is only slightly larger than $2.1\rho_0$ given by the EoS with parameters (5). The final state density is $\rho_{\text{fin}}^1 \approx 5.5\rho_0$, i.e., slightly less than the value $5.9\rho_0$ given by model (5). Thus, the main conclusion is that all the general trends in the behavior of the kaon condensation are the same for both models of the EOS. The critical densities of the s - and p -wave condensations are only slightly higher for the parameters of Eq. (A1).

APPENDIX B: NONEQUILIBRIUM GREEN'S FUNCTIONS

Two-point (2P) functions (a Green's function or a self-energy) are introduced within the Schwinger-Baym-Kadanoff-Keldysh (SBKK) approach as, see Ref. [64],

$$iF(x,y) = \begin{pmatrix} iF^{--}(x,y) & iF^{-+}(x,y) \\ iF^{+-}(x,y) & iF^{++}(x,y) \end{pmatrix} = \begin{pmatrix} \langle \mathcal{T} \hat{A}(x) \hat{B}(y) \rangle & \mp \langle \hat{B}(y) \hat{A}(x) \rangle \\ \langle \hat{A}(x) \hat{B}(y) \rangle & \langle \mathcal{T}^{-1} \hat{A}(x) \hat{B}(y) \rangle \end{pmatrix}, \quad (\text{B1})$$

where \mathcal{T} and \mathcal{T}^{-1} are the usual time and antitime ordering operators. Note that in notations of Ref. [65], in contrast to the Green's functions, the “ \pm, \mp ” self-energies would have an extra sign “ $-$,” since they contain the vertices $V^- = -iV_0$ and $V^+ = +iV_0$. Not all four components of F are independent. The useful Kubo-Schwinger-Martin relations among them can be found in Ref. [64].

We denote the fermionic Green's functions and self-energies by $\hat{G}^{i,j}$ and $\hat{\Sigma}^{i,j}$, respectively, and the bosonic ones as $D^{i,j}$ and $\Pi^{i,j}$ with $i,j = \pm$. The hats on the fermionic 2P functions point on their spin structure, e.g., $\hat{G}^{R,A} = [\hat{p} - m_f - \hat{\Sigma}^{R,A}(p)]^{-1}$. For systems in equilibrium, the “ $-+$ ” Green's functions are connected to the spectral functions and occupation numbers by the Kubo-Schwinger-Martin relations

$$i\hat{G}^{-+}(p) = -\hat{A}_f(p)n^f(\epsilon), \quad i\hat{G}^{+-}(p) = \hat{A}_f(p)[1 - n^f(\epsilon)],$$

$$iD^{-+}(p) = A_b(p)n^b(\epsilon), \quad iD^{+-}(p) = A_b(p)[1 + n^b(\epsilon)], \quad (\text{B2})$$

$$i\hat{\Sigma}^{-+}(p) = \hat{\gamma}_f(p)n^f(\epsilon), \quad i\hat{\Sigma}^{+-}(p) = -\hat{\gamma}_f(p)[1 - n^f(\epsilon)],$$

$$i\Pi^{-+}(p) = -\gamma_b(p)n^b(\epsilon),$$

$$i\Pi^{+-}(p) = -\gamma_b(p)[1 + n^b(\epsilon)], \quad (\text{B3})$$

where $\hat{A}_f(p) = -2\text{Im}\hat{G}_f^R(p)$, $A_b(p) = -2\text{Im}D_b^R(p)$ are the fermion and the boson spectral functions, $\hat{\gamma}_f(p) = -2\text{Im}\hat{\Sigma}_f^R(p)$, $\gamma_b = -2\text{Im}\Pi_b^R$ are the corresponding widths, and

$$n^{f,b}(\epsilon) = \{\exp[(\epsilon - \mu_{f,b})/T] \pm 1\}^{-1} \quad (\text{B4})$$

are the fermion/boson occupation numbers, and $\mu_{f,b}$ stands for the fermionic and bosonic chemical potentials.

In the quasiparticle approximation ($\gamma_b \rightarrow 0$ in the bosonic Green's functions), we have

$$\begin{aligned} A_b(q) &\approx 2\pi\delta[q_0^2 - \vec{q}^2 - m_b^2 - \text{Re}\Pi^R(q_0, \vec{q})] \\ &= \sum_i 2\pi Z_q^{b,i} \delta(q_0 - \omega_b^i(\vec{q})), \end{aligned} \quad (\text{B5})$$

$$\text{Re}D_b^R(q) \approx \sum_i \frac{Z_q^{b,i}}{q_0 - \omega_b^i(\vec{q})},$$

where $Z_q^{b,i} = 1/[2q_0 - \partial\text{Re}\Pi^R/\partial q_0]_{q_0 = \omega_b^i(\vec{q})}$ are the quasiparticle normalization factors corresponding to a given spectrum branch $\omega_b^i(\vec{q})$.

As a step towards the nonrelativistic limit, it is convenient to approximate the spin structure of the fermionic Green's functions as $\hat{G}_f^R(p) = (\not{p} + m_f)G_f^R(p)$ and $\hat{A}_f(p) = (\not{p} + m_f)A_f(p)$. In the quasiparticle approximation ($\gamma_f \rightarrow 0$), we have

$$A_f(p) \approx 2\pi\delta[\epsilon^2 - \epsilon_0^2(\vec{p}) - \text{Re}\Sigma^R(\epsilon, \vec{p})] = Z_p^f \frac{\pi}{\epsilon_p^-} \delta(\epsilon - \epsilon_p^-), \quad (\text{B6})$$

$$\text{Re}G_f^R(\epsilon, \vec{p}) \approx \frac{1}{2\epsilon_p^-} \frac{Z_p^f}{\epsilon - \epsilon_p^-}, \quad Z_p^f = [1 - \partial\text{Re}\Sigma^R/\partial\epsilon^2|_{\epsilon = \epsilon_p^-}]^{-1},$$

where ϵ_p^- obeys the dispersion equation $\epsilon_p^2 = \epsilon_0^2(\vec{p}) + \text{Re}\Sigma^R(\epsilon_p^-, \vec{p})$ with $\epsilon_0(\vec{p}) = \sqrt{m_f^2 + \vec{p}^2}$. The self-energy Σ^R includes averaging over the spin structure $\Sigma^R = \frac{1}{2}\text{Tr}\{\hat{\Sigma}^R \cdot (\not{p} + m_f)\}$.

The mean-field solutions (3) of the equation of motion for a baryon B , following from Eq. (2), can be parametrized by the self-energy $\Sigma^R(\epsilon, \vec{p}) = 2V_B\epsilon + V_B^2 - 2m_{NG}\sigma + g_{\sigma B}^2\sigma^2$. Then, we have $\epsilon_p^- = E_B(\vec{p})$, with $E_B(\vec{p})$ defined in Eq. (3) and $Z_p^B = [1 - V_B/E_B(\vec{p})]^{-1} = 1 + V_B/\epsilon_B(\vec{p}) \approx 1$.

APPENDIX C: EVALUATION OF FLUCTUATION TERMS

We will estimate fluctuation effects to the baryon self-energies and the feedback from the in-medium kaon modification to the polarization operator.

1. Correction of the baryon Green's functions due to kaon fluctuations

In Refs. [19,20,39–41,43], it has been argued that fluctuation contributions to the hyperon self-energy are essential at low densities and at kaon energies not far away from the mass shell. This is, mainly, due to the presence of dynamically generated $\Lambda(1405)$ resonance close to the kaon-nucleon threshold. This resonance dominates the s -wave kaon polarization operator at $\omega \sim m_K$ and it is very sensitive to the Pauli-blocking effect and to the modification of the kaon spectral density. At lower kaon frequencies, corresponding to our main interest, the influence of the $\Lambda(1405)$ resonance is small. Thus, what remains to be analyzed are the self-energy contributions of $\Lambda(1116)$, $\Sigma(1195)$, and $\Sigma^*(1385)$ resonances. Here, we demonstrate that in the low energy region and at baryon densities of our interest these contributions are rather suppressed.

Let us first show this on the example of the diagram

$$\Sigma = \begin{array}{c} \text{K} \\ \text{H} \text{---} \text{---} \text{H} \\ \text{N} \end{array} \quad (\text{C1})$$

This is the self-energy insertion to the full hyperon Green's function due to the KN intermediate states. In Eq. (C1), we draw the full vertices. The nucleon line represents the full Green's function. To be specific, let us concentrate on the kaon-proton self-energy insertion for the Λ hyperon. This corresponds to $H = \Lambda$, $K = K^+$ (according to selected arrow direction), $N = p$ in diagram (C1).

Within the SBKK diagram technique, using the relations between the retarded and “–, +” Green's functions and the self-energies, we obtain

$$\begin{aligned} -i\hat{\Sigma}^R(p) &= \int \hat{V}[\hat{G}^{-+}(p+q)D^R(q) + \hat{G}^R(p+q)D^{-+}(q) \\ &\quad - i\hat{G}^{-+}(p+q)2\text{Im}D^R(q) \\ &\quad + \hat{G}^R(p+q)D^R(q)]\hat{V} \frac{d^4q}{(2\pi)^4}. \end{aligned} \quad (\text{C2})$$

Here, $-i\hat{V} = -i\hat{V}_0\Gamma$ and $-i\hat{V}_0$ are the full and bare “–” vertices, and $i\hat{V} = i\hat{V}_0\Gamma$, $i\hat{V}_0$ are the corresponding “+” vertices, Γ is a scalar form factor, which includes short-range nucleon-baryon correlations and simulates, thereby, the difference between the bare and the full vertices. The last term in Eq. (C2) vanishes, since both retarded Green's functions have their poles in the same complex q_0 semiplane.

To separate the contributions from particles K^+ and anti-particles K^- , we may use the following decompositions for the retarded Green's functions and the Wigner's densities

$$D^R(q) = \theta(q_0)D_{K^+}^R(q) + \theta(-q_0)D_{K^-}^A(-q), \quad (\text{C3})$$

$$D^{-+}(q) = \theta(q_0)D_{K^+}^{-+}(q) + \theta(-q_0)D_{K^-}^{+-}(-q). \quad (\text{C4})$$

This allows us to reduce the integration over q_0 in Eq. (C2) to positive values only. For the Λ self-energy, we have

$$\begin{aligned} \Sigma^R(p) = & \frac{1}{2} \text{Tr} \{ \hat{\Sigma}^R(\not{p} + m_\Lambda^*) \} = \int \frac{d^4 q \theta(q_0)}{(2\pi)^4} 2m_\Lambda^* \bar{V}^2 \{ iG^{-+}(p \\ & + q) [D_{K^+}^R(q) - 2i \text{Im} D_{K^+}^R(q)] + G^R(p \\ & + q) iD_{K^+}^{-+}(q) + iG^{-+}(p - q) [D_{K^-}^R(q) \\ & - 2i \text{Im} D_{K^-}^R(q)] + G^R(p - q) iD_{K^-}^{-+}(q) \}, \end{aligned} \quad (\text{C5})$$

where we used the notations

$$\begin{aligned} \bar{V}^2 = & \bar{V}_0^2 \Gamma^2(q), \quad \bar{V}_0^2 \\ = & C_{K\Lambda}^2 \frac{1}{2} \text{Tr} \left\{ \frac{(\not{p} + m_\Lambda^*)}{2m_\Lambda^*} \not{q} \gamma_5 \frac{(\not{p} - \not{q} + m_N^*)}{2m_N^*} \not{q} \gamma_5 \right\}. \end{aligned} \quad (\text{C6})$$

Having in mind that we are interested in the self-energy insertion to the $\Lambda - p^{-1}$ loop, after expanding the denominators of the fermionic Green's functions near the poles, and assuming that fermions are nonrelativistic, we may insert $(pq) \approx m_N^* \omega$, $p^2 \approx m_N^{*2}$, and $\omega, |\vec{q}|, (m_\Lambda^* - m_N^*) \ll m_\Lambda^*, m_N^*$. As a result, we obtain at the nonrelativistic p -wave vertex $V_0^2 \approx v_0^2 \vec{q}^2$, with $v_0^2 = C_{K\Lambda}^2 m_N^*/m_\Lambda^* \approx (0.3-0.5)/m_\pi^2$. For Σ hyperon, we would have $v_0^2 = C_{KN\Sigma}^2 m_N^*/m_\Sigma^* \approx (0.07-0.09)/m_\pi^2$, and for Σ^* the corresponding coupling is $v_0^2 = \frac{2}{3} C_{KN\Sigma^*}^2 m_N^*/m_{\Sigma^*}^* \approx (0.3-0.5)/m_\pi^2$.

To evaluate $\text{Im}\Sigma^R$ and $\text{Re}\Sigma^R$, we use the quasiparticle approximation for the spectral functions (B6). As we shall see below, nonquasiparticle corrections to the intermediate fermion Green's functions, although exist, produce small contributions to the self-energies at the kaon energies of interest.

We first evaluate $\text{Im}\Sigma^R$. Using Eqs. (B2), (B5), and (B6), we get from Eq. (C2)

$$\begin{aligned} \frac{\text{Im}\Sigma^R(\epsilon, \vec{p})}{2m_\Lambda^*} = & - \sum_i \frac{1}{2} \int \frac{d^3 q}{(2\pi)^2} v_0^2 \vec{q}^2 \Gamma^2 \{ Z_q^{K^-,i} [1 \\ & - n_{p-q}^p] \delta(\Delta_-^i(\epsilon, \vec{p}, \vec{q})) \\ & + Z_q^{K^+,i} n_{p+q}^p \delta(\Delta_+^i(\epsilon, \vec{p}, \vec{q})) \}, \\ & \times \Delta_\pm^i(\epsilon, \vec{p}, \vec{q}) = \epsilon \pm \omega_{K^\pm}(\vec{q}) - E_p(\vec{p} \pm \vec{q}), \end{aligned} \quad (\text{C7})$$

where i runs over all the K^- and K^+ branches. Here, $\omega_K^i(\vec{q})$ are functions of \vec{q}^2 and $n_p^p = \theta(p_{F,p} - |\vec{p}|)$ is the proton occupation function. We used also that occupations of real K^+ and K^- mesons are absent at $T=0$ (we do not consider here the processes on the kaon condensate field).

In the region interesting for us, $\omega_{K^-} \approx E_\Lambda(0) - E_p(0)$, the δ functions in Eq. (C7) allow only for the contribution of the lowest branch of the K^- spectrum.

Further evaluation can be easily done for $\vec{p}=0$. For positive ϵ , the imaginary part differs from zero only for $\epsilon > \omega_{K^-}(0) + E_p(0)$, and it is equal to

$$\frac{\text{Im}\Sigma^R(\epsilon, 0)}{2m_\Lambda^*} = - \frac{v_0^2}{4\pi\alpha} Z_q^{K^-} \Gamma^2(\vec{q}) \vec{q}^3 \theta(\vec{q} - p_{F,p}), \quad (\text{C8})$$

where \vec{q} is a solution of the equation $\Delta_-(\epsilon, 0, \vec{q}) = 0$ and $\alpha = -\partial\Delta_-(\epsilon, 0, \vec{q})/\partial\vec{q}^2|_{\vec{q}^2=\vec{q}^2} > 0$. If \vec{q} is small, namely,

$$-\Delta_-(\epsilon, 0, 0) \frac{\partial\Delta_-(\epsilon, 0, q)}{\partial\vec{q}^2} \Big|_{\vec{q}^2=0} \ll 1,$$

we may approximate $\vec{q} \approx \vec{q}_0 = \sqrt{\Delta_-(\epsilon, 0, 0)/\alpha_0}$, where

$$\alpha_0 = - \frac{\partial\Delta_-(\epsilon, 0, q)}{\partial\vec{q}^2} \Big|_{\vec{q}^2=0}.$$

From the θ function in Eq. (C8), it follows that the fluctuations contribute to the imaginary part of the given diagram only, if $\epsilon > \omega_{K^-}(0) + E_p(0) + p_{F,p}^2$.

From Fig. 15, we see that $\omega_{K^-}(\vec{q})$ is a very flat function of \vec{q}^2 , and we can, therefore, neglect the momentum dependence of the K^- spectrum for $0 < |\vec{q}| \leq 2 m_\pi$. The imaginary part of the diagram at finite \vec{p} is

$$\begin{aligned} \frac{\text{Im}\Sigma^R(\epsilon, \vec{p})}{2m_\Lambda^*} = & -v_0^2 \int \frac{|\vec{p}| + \vec{q}_0}{||\vec{p}| - \vec{q}_0|} \frac{d|\vec{q}||\vec{q}|^3}{4\pi|\vec{p}|} Z_q^{K^-} \Gamma^2[m_N^* \\ & + \Delta_-(\epsilon, 0, 0)] \theta[\Delta_-(\epsilon, p_{F,p}, 0)] \\ \approx & - \frac{v_0^2 m_N^*}{2\pi} Z_{q_0}^{K^-} \Gamma^2(\vec{q}_0) \vec{q}_0 (\vec{q}_0^2 + \vec{p}^2) \\ & \times \theta[\Delta_-(\epsilon, p_{F,p}, 0)]. \end{aligned}$$

The energy and momentum of the Λ within the Λp^{-1} loop, contributing to the K^- polarization operator at $|\vec{q}|=0$ are $\epsilon = E_p(\vec{p}) + \omega_{K^-}(0)$ and $|\vec{p}| \leq p_{F,p}$. Therefore, the conditions for nonzero θ functions in Eqs. (C8 and C9) are not fulfilled within the momentum integration interval of the Λp^{-1} loop.

For $\text{Re}\Sigma^R$, using Eqs. (B2), (B6), (C3), and (C6), we get from Eq. (C2)

$$\begin{aligned} \frac{\text{Re}\Sigma^R(\epsilon, \vec{p})}{2m_\Lambda^*} = & - \sum_i \int \frac{d^3 \vec{q}}{(2\pi)^3} v_0^2 \vec{q}^2 \Gamma^2 \left\{ \frac{n_{p-q}^p Z_q^{K^-,i}}{\Delta_-^i(\epsilon, \vec{p}, \vec{q})} \right. \\ & \left. + \frac{n_{p+q}^p Z_q^{K^+,i}}{\Delta_+^i(\epsilon, \vec{p}, \vec{q})} \right\}. \end{aligned} \quad (\text{C9})$$

For relevant ϵ , the main contribution is given by the first term with the lowest K^- branch. For $|\vec{p}|=0$ the integral in Eq. (C9) is determined by $|\vec{q}|\sim\bar{q}$, and we can expand $\Delta_-(\epsilon,0,\vec{q})\approx\alpha(\bar{q}^2-\bar{q}^2)$. If $Z_q^{K,i}$ and Γ depend weakly on the momentum, the remaining integration is straightforward and gives

$$\frac{\text{Re}\Sigma^R(\epsilon,0)}{2m_\Lambda^*}\approx\frac{v_0^2\Gamma^2(\bar{q})Z_q^{K-}}{2\pi^2\alpha}\left[\frac{p_{F,p}^3}{3}+\bar{q}^2p_{F,p}-\bar{q}^2|\bar{q}|\frac{1}{2}\ln\left|\frac{|\bar{q}|+p_{F,p}}{|\bar{q}|-p_{F,p}}\right|\right]. \quad (\text{C10})$$

The extension for finite \vec{p} can be easily done if we neglect the \vec{q} dependence of the kaon spectrum. This is justified by our numerical analysis for $|\vec{q}|\lesssim 2m_\pi$. Then, $\Delta_-(\epsilon,\vec{p}-\vec{q},0)\approx[\bar{q}_0^2-(\vec{p}-\vec{q})^2]/2m_N^*$, and the integration gives

$$\frac{\text{Re}\Sigma^R(\epsilon,\vec{p})}{2m_\Lambda^*}\approx\frac{v_0^2m_N^*}{\pi^2}\Gamma^2(\bar{q}_0)Z_{q_0}^{K-}\left[\frac{p_{F,p}^3}{3}+(\bar{q}_0^2+\vec{p}^2)p_{F,p}-(\bar{q}_0^2+\vec{p}^2)|\bar{q}_0|\frac{1}{2}\ln\left|\frac{|\bar{q}_0|+p_{F,p}}{|\bar{q}_0|-p_{F,p}}\right|\right]. \quad (\text{C11})$$

Now, we estimate the real part of the hyperon self-energy at $\vec{p}=0$ and $\epsilon=E_p(0)+\omega_{K^-}(0)$. We have $\bar{q}_0\rightarrow 0$ and

$$\frac{\text{Re}\Sigma^R}{2m_\Lambda^*}\approx c\equiv v_0^2m_N^*\Gamma^2(0)Z_0^{K-}\rho_p\sim 0.3m_\pi\Gamma^2(0)\frac{\rho_p}{\rho_0},$$

with $m_N^*\approx 0.6m_N$ and $Z_0^{K-}=Z_{\bar{q}=0}^{K-}\sim 1/[2\omega_{K^-}(0)]\sim 1/(2\mu_e)$. Assuming that the modification of the p -wave $KN\Lambda$ vertex is determined by the graphical equation (66) with Λp^{-1} intermediate states, we can use the corresponding part of Eq. (68) and write

$$\Gamma(0)\approx\frac{1}{1-f'_\Lambda C_0\Phi_{p\Lambda}(\omega_{K^-}(0),0)}.$$

The Lindhard function can be estimated as

$$\Phi_{p\Lambda}(\omega_{K^-}(0),0)\approx\frac{2m_N^*\rho_p}{\Delta_{p\Lambda}^-(\omega_{K^-}(0),0,p_{F,p})}\approx\frac{\rho_p}{\Delta}, \quad (\text{C12})$$

where $\Delta=\omega_{K^-}(0)-E_\Lambda(0)+E_p(p_{F,p})$. The value of $E_\Lambda(0)-E_p(p_{F,p})$ can be estimated from Fig. 5 where this is shown by the dashed-dotted line. We estimate $\Delta\sim -m_\pi$ and therefore, $\Phi_{p\Lambda}\sim -0.5m_\pi^2\rho_p/\rho_0$. Thus, we obtain $\Gamma(0)\approx 1/(1+0.3\rho_p/\rho_0)$ and

$$\text{Re}\Sigma^R/(2m_\Lambda^*)\lesssim 0.2m_\pi, \quad (\text{C13})$$

for $\rho_p\lesssim 3\rho_0$. We conclude that the absolute value of the fluctuation contribution is small for $\vec{p}\rightarrow 0$ and this can be mimicked by a variation of the weakly constrained parameters of Lagrangian (2).

From Eqs. (C10) and (C11), one can see that $\text{Re}\Sigma^R$ is logarithmically divergent at $|\vec{p}|\rightarrow p_{F,p}$ when $\bar{q}\rightarrow p_{F,p}$. In order to analyze which effects this can produce for the Λp^{-1} contribution to the polarization operator, we separate the leading divergent term

$$\left(\frac{\text{Re}\Sigma^R}{2m_\Lambda^*}\right)_{\text{div}}\approx v_0^2m_N^*\Gamma^2(p_{F,p})Z_{p_{F,p}}^{K-}\frac{p_{F,p}^3}{\pi^2}\ln\frac{p_{F,p}-|\vec{p}|}{p_{F,p}}\approx 3c\ln\frac{p_{F,p}-|\vec{p}|}{p_{F,p}}, \quad (\text{C14})$$

and estimate the variation of the Lindhard function (29):

$$\delta\Phi_{p\Lambda}\approx\int_0^{p_{F,p}}d|\vec{p}||\vec{p}|^2\left[\frac{1}{\Delta-3c\ln(1-p/p_{F,p})}-\frac{1}{\Delta}\right].$$

Using Eq. (C12), we write

$$\delta\Phi_{p\Lambda}/\Phi_{p\Lambda}\approx F(3c/\Delta),$$

$$F(a)=a\int_0^1dx(1-x)^2/(1-a\ln x), \quad (\text{C15})$$

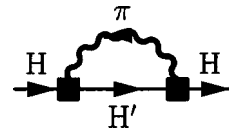
and find

$$|\delta\Phi_{p\Lambda}/\Phi_{p\Lambda}|\lesssim 0.2 \text{ for } |3c/\Delta|\lesssim 0.6.$$

The above estimations prove that the self-energy corrections of the Λ propagator induced by the kaon fluctuations [diagram (C1)] do not modify the properties of K^- excitations with small energies and momenta, which we consider in the main part of this paper. The same estimation can be done also for the \bar{K}^0n contribution to the Λ self-energy and for the Σ and Σ^* self-energies.

2. Correction of the baryon Green's functions due to pion fluctuations

There is another type of diagrams



(C16)

relating to pion fluctuations. Pions are softened in the nucleon matter already at densities $\sim\rho_0$. The softening effect may result in pion condensation at densities $\rho>\rho_{c\pi}$, where the critical density for pion condensation $\rho_{c\pi}$ might be smaller than that for the kaon condensation [66,21]. However, in this work, we concentrate only on kaon polarization effects. Thus, we disregard such a possibility assuming $\rho<\rho_{c\pi}$.

The main contribution to Eq. (C16) comes from the width of soft pions due to the Landau damping. The maximum of the pion spectral function is achieved at a small pion energy $q_0 < m_\pi$ and a finite momentum $|\vec{q}| = |\vec{q}_m|$. In the diagram with the π^0 intermediate states the typical momenta of hyperons are $\sim p_{F_n}$ for Hn^{-1} loops in the the K^- polarization operator or $\sim p_{F_p}$ for the Hp^{-1} loops. With a simplifying assumption $|\vec{q}_m| \ll 2p_{F_n}, 2p_{F_p}$, the nucleon Green's function can be factorized out from the integral. The result is then reduced to the calculation of a pionic tadpole [67]



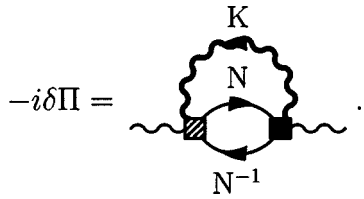
$$(C17)$$

At zero temperature, the in-medium contributions from pion fluctuations given by Eq. (C17) are numerically small for all densities except in the closest vicinity of the pion condensation critical point [67,21]. For finite temperatures such contributions are substantially increased [68].

The fermion self-energy insertions discussed here enter the loop diagrams of the kaon polarization operator. Since we found them to be rather small, we may still work with the quasiparticle fermion Green's functions in the hyperon-nucleon-hole loop diagrams treating fermions on the mean-field level, as we did it in main part of the text.

3. Fluctuation contributions to the K^- polarization operator

One of the important fluctuation processes in the kaon polarization operator is given by the diagram



$$(C18)$$

The diagram with free vertices was extensively discussed in the context of kaonic atoms [19,20]. In Ref. [19] both vertices were taken constants and equal to $V_0 \approx 4\pi(1 + m_K/m_N)\sqrt{(a_{KN}^{I=0})^2 + 3(a_{KN}^{I=1})^2}$ for isospin-symmetrical case, where a_{KN}^I is the $\bar{K}N$ scattering length for isospin I . In the threshold region, a large value of the vertex $V_0 \sim 4\pi/m_\pi$ was obtained. We will also use the energy-independent bare vertex (hatched box) but estimate V_0 using our amplitudes of Figs. 2 and 3 in the far off-mass-shell region. In this energy region, $V_0 \sim 1/m_\pi$, i.e., a much smaller value than that in the threshold region. Accordingly, we expect a significant suppression of the contribution from this diagram to the kaon polarization operator. Another suppression comes from short-range correlations taken into account in the full box (right vertex).

From Eq. (C18), we obtain the advanced polarization operator

$$\begin{aligned} \delta\Pi^A(k) = & \int [-i\mathcal{P}^{+-}(k+q)D^A(q) + \mathcal{P}^A(k+q)iD^{+-}(q) \\ & - \mathcal{P}^{+-}(k+q)2\text{Im}D^A(q) \\ & + i\mathcal{P}^A(k+q)iD^A(q)] \frac{d^4q}{(2\pi)^4}, \end{aligned} \quad (C19)$$

where \mathcal{P} corresponds to the NN^{-1} loop (including vertices). The last term in Eq. (C19) is zero.

Let us consider first the real part of the diagram. Using Eqs. (B2), (B3), we obtain

$$\begin{aligned} \delta\text{Re}\Pi^A(k) = & \int \{[1 + n^K(k_0 - q_0)]\gamma_p(k - q)\text{Re}D^A(-q) \\ & + [1 + n^K(q_0)]A_K(q)\text{Re}\mathcal{P}^A(k + q)\} \frac{d^4q}{(2\pi)^4}, \end{aligned} \quad (C20)$$

where $\gamma_p = 2\text{Im}\mathcal{P}^A$ and in the first term we have replaced $q \rightarrow -q$. Using relations $1 + n_{-q_0}^b = -n_{q_0}^b$ and (C3), we reduce the integration in Eq. (C20) to the positive energies:

$$\begin{aligned} \delta\text{Re}\Pi^A(k) = & \int \frac{d^4q}{(2\pi)^4} \theta(q_0) \{ [1 + n^K(k_0 - q_0)] \\ & \times \gamma_p(k - q)\text{Re}D_{K^-}^A(-q) + [1 + n^K(k_0 + q_0)] \\ & \times \gamma_p(k + q)\text{Re}D_{K^+}^A(q) + [1 + n^K(q_0)]A_{K^+}(q) \\ & \times \text{Re}\mathcal{P}^A(k + q) + n^K(q_0)A_{K^-}(q)\text{Re}\mathcal{P}^A(k - q) \}. \end{aligned} \quad (C21)$$

The NN^{-1} loop is suppressed at large frequencies $\omega > |\vec{k}|v_{F,N} + \vec{k}^2/2m_N^*$. Therefore, the second and the third terms give a small contribution in the energy region of our interest. The fourth term is identically zero [$n^K(q_0) = 0$ for $q_0 > 0$ at $T = 0$]. Thus, we may keep only the first term in Eq. (C21)

$$\begin{aligned} \delta\text{Re}\Pi^A(k) \approx & \int \frac{d^4q}{(2\pi)^4} \theta(q_0) V_0^2 \Gamma^2 [1 + n^K(k_0 - q_0)] \\ & \times \gamma_0(k - q)\text{Re}D_{K^-}^A(-q). \end{aligned} \quad (C22)$$

Here, we introduced $\gamma_p = V_0^2 \Gamma^2 \gamma_0$, using the fact that the correlation factor Γ is expressed through the Lindhard function Φ^A , which leads to a Γ^2 factor. In the spacelike region, $\gamma_0(k) = \gamma_0(k_0, \vec{k})$ has a compact analytic presentation [69], which at $T = 0$ gives

$$\gamma_0(k_0, \vec{k}) = \frac{m_N^{*2} k_0}{2\pi|\vec{k}|}, \quad 0 < k_0 < \Omega_-(\vec{k}), \quad (C23)$$

$$\begin{aligned}\gamma_0(k_0, \vec{k}) &= \frac{m_N^{*3}}{4\pi|\vec{k}|^3} [\Omega_-(\vec{k}) + k_0] [\Omega_+(\vec{k}) - k_0], \\ 0 < \Omega_-(\vec{k}) < k_0 < \Omega_+(\vec{k}), \quad (C24) \\ \Omega_{\pm}(\vec{k}) &= \frac{2|\vec{k}|p_{F,N} \pm \vec{k}^2}{2m_N^*}.\end{aligned}$$

Let us discuss the low energy contribution (C23) to the polarization operator which we label below by subscript ‘‘1.’’ The q_0 integration is easily done using

$$\max(\nu, 0) < q_0 < k_0, \quad \nu = k_0 - \Omega_-(\vec{k} - \vec{q}).$$

We obtain

$$\begin{aligned}\text{Re}\delta\Pi_1^A(k) &\approx \frac{V_0^2 m_N^{*2}}{(2\pi)^2} \int_{|\vec{k}-\vec{q}| < 2p_{F,N}} \frac{d^3\vec{q}}{(2\pi)^3} \frac{\Gamma^2 Z_q^{K^-}}{|\vec{k}-\vec{q}|} \\ &\times \left[[k_0 - \omega_{K^-}(\vec{q})] \ln \frac{[k_0 - \omega_{K^-}(\vec{q})]}{\max(\nu, 0) - \omega_{K^-}(\vec{q})} \right. \\ &\left. - k_0 + \max(\nu, 0) \right]. \quad (C25)\end{aligned}$$

This contribution can be easily estimated for $|k_0 - \omega_{K^-}(0)|/k_0 \ll \omega_{K^-}(0)$ and $\vec{k}=0$. We note that due to the flatness of the kaon spectrum $\omega_{K^-}(\vec{q}) \approx \omega_{K^-}(0)$. Hence, for $k_0 \sim \omega_{K^-}(0)$, we can neglect the first term in Eq. (C25). Then,

$$\begin{aligned}\text{Re}\delta\Pi_1^A(k_0, 0) &\approx -\frac{V_0^2 m_N^{*2}}{(2\pi)^2} \\ &\times \int_0^{2p_{F,N}} \frac{d|\vec{q}||\vec{q}|}{2\pi^2} \Gamma^2 Z_q^{K^-} \min(k_0, \Omega_-(\vec{q})). \quad (C26)\end{aligned}$$

For $k_0 \sim \omega_{K^-}(0) > p_{F,N}^2/(2m_N^*)$ there is always $k_0 > \Omega_-(\vec{q})$, and we find

$$\text{Re}\delta\Pi_1^A(k_0, 0) \approx -\frac{V_0^2 m_N^{*2}}{4\pi^2} \Gamma^2(0) Z_0^{K^-} \rho_N p_{F,N} \equiv -\frac{C p_{F,N}}{4\pi^2}. \quad (C27)$$

For $k_0 \sim \omega_{K^-}(0) < p_{F,N}^2/(2m_N^*)$, the inequalities $k_0 > \Omega_-(\vec{q})$ or $k_0 < \Omega_-(\vec{q})$ together with $0 < |\vec{q}| < 2p_{F,N}$ determine three regions for momentum integration,

$$\begin{aligned}\text{Re}\delta\Pi_1^A(k_0, 0) &\approx -\frac{V_0^2 m_N^{*2}}{(2\pi)^2} \Gamma^2(0) Z_0^{K^-} \left[\left(\int_0^{q_-(k_0)} \right. \right. \\ &\left. \left. + \int_{q_+(k_0)}^{2p_{F,N}} \right) \frac{d|\vec{q}||\vec{q}|}{2\pi^2} \Omega_-(\vec{q}) + \int_{q_-(k_0)}^{q_+(k_0)} \frac{d|\vec{q}||\vec{q}|}{2\pi^2} k_0 \right],\end{aligned}$$

bordered by $q_{\pm}(k_0) = p_{F,N} \pm \sqrt{p_{F,N}^2 - 2m_N^* k_0}$ which follows from the equation $k_0 = \Omega_-(q_{\pm})$. The integration results in

$$\text{Re}\delta\Pi_1^A(k_0, 0) \approx -\frac{C p_{F,N}}{4\pi^2} \left[1 - \left(1 - \frac{2k_0 m_N^*}{p_{F,N}^2} \right)^{3/2} \right]. \quad (C28)$$

Now, we discuss the contribution from the energy region (C24) which we indicate by subscript ‘‘2.’’

$$\begin{aligned}\text{Re}\delta\Pi_2^A(k_0, 0) &\approx \frac{V_0^2 m_N^{*3}}{(2\pi)^4} \int_0^{2p_{F,N}} \frac{d|\vec{q}|}{|\vec{q}|} \Gamma^2 Z_q^{K^-} \theta(k_0 - \Omega_-(\vec{q})) \\ &\times \int_{k_0 - \Omega_+(\vec{q})}^{k_0 - \Omega_-(\vec{q})} dq_0 \\ &\times \frac{[\Omega_-(\vec{q}) + k_0 - q_0][\Omega_+(\vec{q}) - k_0 + q_0]}{q_0 - \omega_{K^-}}.\end{aligned}$$

For $k_0 \sim \omega_{K^-}(0)$ and $\vec{k}=0$ this contributes to

$$\begin{aligned}\text{Re}\delta\Pi_2^A(k_0, 0) &\approx \frac{V_0^2 m_N^{*3}}{(2\pi)^4} \int_0^{2p_{F,N}} \frac{d|\vec{q}|}{|\vec{q}|} \Gamma^2 Z_q^{K^-} \\ &\times \theta(k_0 - \Omega_-(\vec{q})) \left[\Omega_-(\vec{q}) \Omega_+(\vec{q}) \ln \frac{\Omega_-(\vec{q})}{\Omega_+(\vec{q})} \right. \\ &\left. - \frac{3}{2} \Omega_-^2(\vec{q}) + 2\Omega_-(\vec{q}) \Omega_+(\vec{q}) - \frac{1}{2} \Omega_+^2(\vec{q}) \right].\end{aligned}$$

We have neglected terms $\propto [k_0 - \omega_{K^-}(\vec{q})]$ in the integrand, since these are small due to the flatness of the K^- spectrum. For $k_0 \sim \omega_{K^-}(0) > p_{F,N}^2/(2m_N^*)$, we find

$$\text{Re}\delta\Pi_2^A(k_0, 0) \approx 3 \frac{C p_{F,N}}{4\pi^2} G(0), \quad (C29)$$

and for $k_0 \sim \omega_{K^-}(0) < p_{F,N}^2/(2m_N^*)$, we have

$$\text{Re}\delta\Pi_2^A(k_0, 0) \approx 3 \frac{C p_{F,N}}{4\pi^2} G(x), \quad x = \sqrt{1 - 2k_0 m_N^*/p_{F,N}^2}. \quad (C30)$$

Here, we introduced functions

$$G(x) = \frac{1}{16} \left(\int_0^{1-x} + \int_{1+x}^2 \right) dt \left[(4-t^2) \ln \frac{2-t}{2+t} - 4t^2 + 4t \right],$$

$$G(0) = -\frac{2}{3}, \quad G(x \rightarrow 1) \approx -\frac{5}{4}(1-x). \quad (\text{C31})$$

The suppression of the nucleon–nucleon-hole loop in the scalar-isoscalar channel can be taken into account as in Ref. [21] [for recent review, see Ref. [70], Eqs. (4)–(8)] $\Gamma = 1/[1 - 2(f+f')C_0 A_{NN}(\omega=0, q=p_{F,N})]$, where A_{NN} is the nucleon–nucleon-hole loop (without the spin degeneracy factor 2), and $A_{NN}(\omega=0, q=p_{F,N}) \approx -m_N p_{F,N}/(2\pi^2)$. The Landau-Migdal parameters of the NN interaction are $f \approx 0$ and $f' \approx 0.5-0.6$ [71]. Thus, we have $\Gamma \sim 1/[1 + 0.3(\rho_N/\rho_0)^{1/3}]$. For $\rho_N \leq (3-5)\rho_0$ we have $C \sim m_\pi$. When $\omega_{K^-}(0) > p_{F,N}^2/(2m_N^*)$, the attractive contribution of diagram (C18) is estimated to be

$$-\text{Re}\delta\Pi^A \leq 0.3m_\pi^2.$$

The $\text{Re}\delta\Pi^A$ remains attractive also for larger densities, when $\omega_{K^-}(0) < p_{F,N}^2/(2m_N^*)$. However, its absolute value is additionally suppressed by the ratio $\omega_{K^-}(0)m_N^*/p_{F,N}^2$.

The imaginary part of the diagram under consideration describes the processes in which a kaon excitation dissolves into multiparticle nucleon–nucleon-hole modes. If the K^- energy meets the electron chemical potential in the region where the imaginary part of this diagram is, the K^- condensation does not occur via a second-order phase transition.

Using Eq. (C19), we obtain

$$\text{Im}\delta\Pi^A = \int \frac{d^4q}{(2\pi)^4} [i\mathcal{P}^{+-}(k+q)\text{Im}D^A(q) + \text{Im}\mathcal{P}^A(k+q)iD^{+-}(q)]. \quad (\text{C32})$$

With the help of relations (B2) and (B3), we find

$$\text{Im}\delta\Pi^A = \int \frac{d^4q}{(2\pi)^4} \frac{1}{2} \gamma_P(k+q) A_K(q) [n^b(q_0) - n^b(k_0+q_0)]. \quad (\text{C33})$$

Using relations $1+n^b(-q_0) = -n^b(q_0)$ and (C3), we reduce the integral in Eq. (C33) to the positive energies:

$$\text{Im}\delta\Pi^A = \int \theta(q_0) \frac{d^4q}{(2\pi)^4} \frac{1}{2} \{ \gamma_P(k+q) A_{K^+}(q) [n^b(q_0) - n^b(k_0+q_0)] + \gamma_P(k-q) A_{K^-}(q) [1+n(q_0) + n(k_0-q_0)] \}. \quad (\text{C34})$$

The second term gives the main contribution. Taking into account that at $T=0$ there is $(1+n_{q_0}^K + n_{k_0-q_0}^K) = \theta(k_0 - q_0)$, we obtain

$$\text{Im}\delta\Pi^A = \frac{\gamma}{2} = \frac{1}{2} \int_0^{k_0} \frac{dq_0}{2\pi} \frac{d^3q}{(2\pi)^3} V_0^2 \Gamma^2 \gamma_0(k-q) A_{K^-}(q). \quad (\text{C35})$$

The K^- spectral function can be presented in the form

$$A_{K^-}(q) = 2\pi Z_q^{K^-} \delta(\omega_0 - \omega_{K^-}(\vec{q})) + \frac{\gamma(q)}{[q_0^2 - m_K^2 - \text{Re}\Pi^A(q)]^2 + \frac{1}{4} \gamma^2(q)}, \quad (\text{C36})$$

where we separated two different contributions: The first term is the ordinary δ function from the spectral branch; the second term is a possible nonquasiparticle contribution, which can be obtained only by the self-consistent solution of Eq. (C35).

Let us now consider the quasiparticle contribution to the spectral function given by the first term in Eq. (C36).

$$\begin{aligned} \gamma(k_0, \vec{k}) = & \int_{|\vec{k}-\vec{q}| < 2p_{F,N}} \frac{d^3q}{(2\pi)^3} \frac{m_N^{*2} V_0^2}{2\pi |\vec{k}-\vec{q}|} \left\{ [k_0 - \omega_{K^-}(\vec{q})] \right. \\ & \times \theta(k_0 - \omega_{K^-}(\vec{q})) \theta(\omega_{K^-}(\vec{q}) + \Omega_-(\vec{k}-\vec{q}) - k_0) \\ & + \frac{m_N^*}{2|\vec{k}-\vec{q}|^2} [\Omega_-(\vec{k}-\vec{q}) + k_0 - \omega_{K^-}(\vec{q})] \\ & \times [\Omega_+(\vec{k}-\vec{q}) - k_0 + \omega_{K^-}(\vec{q})] \theta(k_0 - \Omega_-(\vec{k}-\vec{q}) \\ & \left. - \omega_{K^-}(\vec{q})) \theta(\Omega_+(\vec{k}-\vec{q}) + \omega_{K^-}(\vec{q}) - k_0) \right\}. \end{aligned}$$

As before, we assume that $\omega_{K^-}(\vec{q})$ is a very flat function in \vec{q}^2 . Then, we obtain

$$\begin{aligned} \gamma = & \theta(z) \theta \left(\frac{p_{F,N}^2}{2m_N^*} - z \right) \frac{m_N^{*2} V_0^2}{4\pi^3} z \int_{q_-(z)}^{q_+(z)} Z_q^K \Gamma^2 |\vec{q}| d|\vec{q}| \\ & + \frac{m_N^{*3} V_0^2}{8\pi^3} \int_{-q_-(z)}^{2p_{F,N}} \frac{d|\vec{q}|}{|\vec{q}|} Z_q^K \Gamma^2 [\Omega_-(\vec{q}) + z] [\Omega_+(\vec{q}) - z] \\ \simeq & \theta(z) \theta \left(\frac{p_{F,N}^2}{2m_N^*} - z \right) \frac{m_N^{*2} V_0^2}{2\pi^3} z Z_0^{K^-} \Gamma^2 p_{F,N} \sqrt{p_{F,N}^2 - 2m_N^* z} \\ & + \theta(z) \theta \left(4 \frac{p_{F,N}^2}{m_N^*} - z \right) \frac{m_N^* V_0^2}{32\pi^3} Z_0^{K^-} \Gamma^2 p_{F,N}^4 H(2m_N^* z / p_{F,N}^2), \end{aligned}$$

$$H(x) = \int_{\sqrt{1+x}-1}^2 \frac{dt}{t} [4t^2 - (t^2 - x)^2],$$

$$H(x \rightarrow 0) \approx 4(1+x), H(x \rightarrow 8) \approx \frac{1}{3}(x-8)^2, \quad (\text{C37})$$

where $z = k_0 - \omega_{K^-}(0)$. As follows from the θ functions there is no width for energies $k_0 < \min_{\vec{q}} \{\omega_{K^-}(\vec{q})\} = \omega_{K^-}(\vec{q}_m)$ and for $k_0 < \omega_{K^-}(0)$. The width exists only above the branch. Exactly at the branch, i.e., for $k_0 = \omega_{K^-}(\vec{k})$, the δ -function contributes only for $\vec{k} \neq 0$. Thus, the quasiparticle part of the K^- spectral function generates no width at $\vec{k} = 0$ at the critical point of the second-order phase transition to the s -wave K^- condensation, and $k_0 = \mu_e = \omega_{K^-}(0)$.

At low energies, $k_0 < \omega_{K^-}(\vec{k})$, where the δ -function term does not contribute, there might appear another contribution from the self-consistent solution given by the second term of (C36). In the following, we find this self-consistent solution and demonstrate that the width exists even for $\vec{k} = 0$ affecting the critical condition for the s -wave condensation. In order to avoid rather cumbersome expressions we make several simplifying assumptions. We assume that $k_0 \sim \omega_{K^-}(\vec{k}) \ll \epsilon_{FN}$, and $(\partial \omega_{K^-} / \partial \vec{q}^2)_0$ is very small in the interval $0 < |\vec{q}| < k_0 / v_{FN}$. Then, the spectral function simplifies as

$$A_{K^-}(q_0) \approx \bar{A}(q_0) = \frac{(Z_0^{K^-})^2 \gamma(q_0)}{[q_0 - \omega_{K^-}(0)]^2 + \frac{1}{4} [Z_0^{K^-} \gamma(q_0)]^2}, \quad (\text{C38})$$

and the self-consistent solution of Eq. (C35) for the width γ is determined by

$$\begin{aligned} \gamma(k_0) \approx & \frac{m_N^{*2} V_0^2 \Gamma^2}{8\pi^4} \int_0^{2p_{F,N}} d|\vec{q}| |\vec{q}| \int_0^{\min\{k_0, \Omega_-(\vec{q})\}} dz z \bar{A}(k_0 - z) \\ & + \frac{m_N^{*3} V_0^2 \Gamma^2}{16\pi^4} \int_0^{2p_{F,N}} \frac{d|\vec{q}|}{|\vec{q}|} \int_{\Omega_-(\vec{q})}^{\min\{k_0, \Omega_+(\vec{q})\}} dz [\Omega_-(\vec{q}) \\ & + z] [\Omega_+(\vec{q}) - z] \theta(k_0 - \Omega_-(\vec{q})) \bar{A}(k_0 - z) \\ = & \frac{m_N^{*2} V_0^2 \Gamma^2}{8\pi^4} \left\{ \left[\int_0^{q_-(k_0)} + \int_{q_+(k_0)}^{2p_{F,N}} \right] d|\vec{q}| |\vec{q}| \int_0^{\Omega_-(\vec{q})} dz \right. \\ & + \left. \int_{q_-(k_0)}^{q_+(k_0)} d|\vec{q}| |\vec{q}| \int_0^{k_0} dz \right\} z \bar{A}(k_0 - z) \\ & + \frac{m_N^{*3} V_0^2 \Gamma^2}{16\pi^4} \left[\int_0^{q_-(k_0)} \right. \\ & + \left. \int_{q_+(k_0)}^{2p_{F,N}} \right] \frac{d|\vec{q}|}{|\vec{q}|} \int_{\Omega_-(\vec{q})}^{\min\{k_0, \Omega_+(\vec{q})\}} dz [\Omega_-(\vec{q}) + z] \\ & \times [\Omega_+(\vec{q}) - z] \bar{A}(k_0 - z), \quad (\text{C39}) \end{aligned}$$

where we replaced $q_0 = k_0 - z$. For $k_0 \sim \omega_{K^-} \ll p_{F,N}^2 / 2m_N^*$, we have $q_- \approx k_0 m_N^* / p_{F,N}$ and $q_+ \approx 2p_{F,N} - k_0 m_N^* / p_{F,N}$. Then, Eq. (C39) reduces to

$$\begin{aligned} \gamma(k_0) = & \frac{m_N^{*2} V_0^2 \Gamma^2}{8\pi^4} \left[\left(\int_0^{[k_0 m_N^*] / p_{F,N}} |\vec{q}| d|\vec{q}| \right) \right. \\ & + \left. \int_{2p_{F,N} - [k_0 m_N^*] / p_{F,N}}^{2p_{F,N}} |\vec{q}| d|\vec{q}| \right] \int_0^{[|\vec{q}| p_{F,N}] / m_N^* - \vec{q}^2 / 2m_N^*} dz \\ & + \int_0^{2p_{F,N}} d|\vec{q}| |\vec{q}| \int_0^{k_0} dz \left[z \bar{A}(k_0 - z) + \frac{m_N^{*3} V_0^2 \Gamma^2}{16\pi^4} \right. \\ & \times \left. \left[\int_0^{[k_0 m_N^*] / p_{F,N}} + \int_{2p_{F,N} - [k_0 m_N^*] / p_{F,N}}^{2p_{F,N}} \right] \right. \\ & \times \left. \frac{d|\vec{q}|}{|\vec{q}|} \int_{\Omega_-(\vec{q})}^{\min\{k_0, \Omega_+(\vec{q})\}} dz [\Omega_-(\vec{q}) + z] \right. \\ & \times \left. [\Omega_+(\vec{q}) - z] \bar{A}(k_0 - z) \right]. \end{aligned}$$

To solve this equation, we assume $\gamma(k_0) \approx \alpha k_0$ for small values of k_0 which we consider here. The main contribution comes from the third integral of the first line $\propto k_0$. In the first integral $|\vec{q}| \sim k_0$ and $z \sim k_0$. In the second integral $2p_{F,N} - |\vec{q}| \sim k_0$ and again $z \propto k_0$. Thus, the first two integrals $\propto k_0^2$. In the fourth integral after the replacement $z = |\vec{q}| p_{F,N} / m_N^* - \vec{q}^2 / (2m_N^*) + \xi$, we see that $\xi \sim \vec{q}^2 \sim k_0^2$ and the integral is $\propto k_0^4$. In the fifth integral, besides this replacement, we introduce $|\vec{q}| = 2p_{F,N} - k_0 m_N^* / p_{F,N} + y$ and observe that $\xi \propto y \propto k_0$. This integral is $\propto k_0^2$. Thus, keeping only the third integral, we obtain

$$\begin{aligned} \alpha k_0 \approx & \frac{m_N^{*2} V_0^2}{4\pi^4} (Z_0^{K^-})^2 \Gamma^2 p_{F,N}^2 \\ & \times \int_0^{k_0} \frac{z \alpha(k_0 - z) dz}{[k_0 - z - \omega_{K^-}(0)]^2 + \frac{1}{4} (Z_0^{K^-})^2 \alpha^2 (k_0 - z)^2}, \end{aligned}$$

which has the nontrivial solution

$$\gamma \approx \alpha k_0 \approx m_N^* V_0 \Gamma p_{F,N} k_0 / \pi^2, \quad (\text{C40})$$

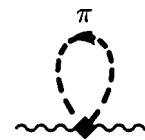
for $\alpha > 2/Z_0^{K^-}$. As one may expect, this inequality indeed holds for rather large densities since $Z_0^{K^-} \sim 1/[2\omega_{K^-}(0)] \gg 1/m_\pi$ for small values $k_0 \sim \omega_{K^-}(0)$.

A principal question is whether there is a width for K^- at low energies. A second-order phase transition with a K^- condensation cannot occur if $\omega_{K^-}(0)$ crosses μ_e in the energy region, where imaginary part of the polarization operator exists. The condensation is possible when the electron chemical potential exceeds $\omega_{K^-}(0)$ reaching the upper border of the region with the width. At least for $\omega_{K^-}(0) > p_{F,N}^2 / (2m_N^*)$, we cannot find self-consistent solution for γ . We would like to stress that a second-order phase transition to the s -wave K^- condensation may not occur only if $\omega_{K^-}(0) = \mu_e < p_{F,N}^2 / (2m_N^*)$. For realistic values of parameters, we have

$\omega_K(0) = \mu_e > p_{Fn}^2 / (2m_N^*)$ and there is no problem for the s -wave K^- condensation.

Thus, the above examples demonstrate that in spite of many new peculiarities associated with the fluctuation processes we may drop the fluctuation contributions for a rough analysis and treat baryons on the mean-field level.

A diagram similar to Eq. (C17) (with kaon lines instead of hyperon lines and a different vertex) describes the $K^- \pi - \pi K^-$ interaction. Within the simplifying assumption for the pion momentum $|\vec{q}_m| \ll 2p_{F,n}$ the diagram is reduced to



(C41)

At zero temperature, the in-medium contribution of pion fluctuations given by Eq. (C41) is numerically small except for a narrow region near the pion condensation critical point [67,21]. For finite temperature such contributions are substantially increased in the vicinity of the pion condensation critical point [68].

-
- [1] R. Stock, Phys. Rep. **135**, 259 (1986); P. Senger and H. Ströbele, J. Phys. G **25**, R59 (1999); H.R. Schmidt and J. Schukraft, *ibid.* **19**, 1705 (1993); W. Reisdorf and H.G. Ritter, Annu. Rev. Nucl. Part. Sci. **47**, 663 (1997).
- [2] D. Röhrich, Nucl. Phys. **A715**, 369c (2003); P. Senger, *ibid.* **685**, 312 (2000).
- [3] V.P. Berezovoy, I.V. Krive, and E.M. Chudnovsky, Sov. J. Nucl. Phys. **30**, 581 (1979).
- [4] D. Kaplan and A. Nelson, Phys. Lett. B **175**, 57 (1986).
- [5] G.E. Brown and H.A. Bethe, Astrophys. J. **423**, 659 (1994).
- [6] E.E. Kolomeitsev, D.N. Voskresensky, and B. Kämpfer, Nucl. Phys. **A588**, 889 (1995).
- [7] G.E. Brown, K. Kubodera, D. Page, and P. Pizzochero, Phys. Rev. D **37**, 2042 (1988); H. Fujii, T. Muto, T. Tatsumi, and R. Tamagaki, Nucl. Phys. **A571**, 758 (1994).
- [8] T. Muto and T. Tatsumi, Phys. Lett. B **283**, 165 (1992); G.E. Brown, V. Thorsson, K. Kubodera, and M. Rho, *ibid.* **291**, 355 (1992).
- [9] G.E. Brown, C.H. Lee, M. Rho, and V. Thorsson, Nucl. Phys. **A567**, 937 (1994); C.H. Lee, G.E. Brown, D.P. Min, and M. Rho, *ibid.* **A585**, 401 (1995).
- [10] V. Thorsson, M. Prakash, and J.M. Lattimer, Nucl. Phys. **A572**, 693 (1994); **A574**, 851(E) (1994).
- [11] N.K. Glendenning and J. Schaffner-Bielich, Phys. Rev. C **60**, 025803 (1999).
- [12] T. Muto, Prog. Theor. Phys. **89**, 415 (1993); H. Yabu, S. Nakamura, F. Myhrer, and K. Kubodera, Phys. Lett. B **315**, 17 (1993).
- [13] T. Muto, Nucl. Phys. **A697**, 225 (2002).
- [14] E.E. Kolomeitsev and D.N. Voskresensky, nucl-th/0001062.
- [15] E.E. Kolomeitsev and D.N. Voskresensky, Phys. Rev. C **60**, 034610 (1999).
- [16] M.F.M. Lutz and E.E. Kolomeitsev, Nucl. Phys. **A700**, 193 (2002).
- [17] E.E. Kolomeitsev, D.N. Voskresensky, and B. Kämpfer, Int. J. Mod. Phys. E **5**, 313 (1996).
- [18] F. Laue *et al.*, Phys. Rev. Lett. **82**, 1640 (1999); C. Sturm *et al.*, J. Phys. G **28**, 1895 (2002).
- [19] M.F.M. Lutz and W. Florkowski, Acta Phys. Pol. B **31**, 2567 (2000); nucl-th/0004020.
- [20] G. Garcia-Recio, J. Nieves, E. Oset, and A. Ramos, Nucl. Phys. **A703**, 271 (2002).
- [21] A.B. Migdal, E.E. Saperstein, M.A. Troitsky, and D.N. Voskresensky, Phys. Rep. **192**, 179 (1990).
- [22] N.K. Glendenning, Astrophys. J. **293**, 470 (1985).
- [23] B. Friedman and V.R. Pandharipande, Nucl. Phys. **A361**, 502 (1981).
- [24] U. Lombardo and W. Zuo, in *Isospin Physics in Heavy-Ion Collisions at Intermediate Energies*, edited by B. A. Li and W. U. Schröder (Nova Science, New York, 2001).
- [25] J. Piekarewicz, preprint, nucl-th/0205007.
- [26] A. Akmal, V.R. Pandharipande, and D.G. Ravenhall, Phys. Rev. C **58**, 1804 (1998).
- [27] J. Schaffner-Bielich and A. Gal, Phys. Rev. C **62**, 034311 (2000).
- [28] N.K. Glendenning and S.A. Moszkowski, Phys. Rev. Lett. **67**, 2414 (1991).
- [29] H. Bandō, T. Motoba, and J. Žofka, Int. J. Mod. Phys. A **5**, 4021 (1990); B.F. Gibson and E.V. Hungerford III, Phys. Rep. **257**, 349 (1995); D.J. Millener, C.B. Dover, and A. Gal, Phys. Rev. C **38**, 2700 (1988).
- [30] C.B. Dover, D.J. Millener, and A. Gal, Phys. Rep. **184**, 1 (1989); C.J. Batty, E. Friedman, and A. Gal, Phys. Lett. B **335**, 273 (1994); J. Mareš, E. Friedman, A. Gal, and B.K. Jennings, Nucl. Phys. **A594**, 311 (1995).
- [31] C.J. Batty, E. Friedman, and A. Gal, Phys. Rev. C **59**, 295 (1999).
- [32] N.K. Glendenning, Phys. Rev. C **64**, 025801 (2001).
- [33] N. Kaiser, P. Siegel, and W. Weise, Nucl. Phys. **A612**, 297 (1997).
- [34] B. Krippa, Phys. Rev. C **58**, 1333 (1998); B. Krippa and J.T. Londergan, *ibid.* **58**, 1634 (1998).
- [35] E. Oset and A. Ramos, Nucl. Phys. **A635**, 99 (1998).
- [36] J.A. Oller and U.-G. Meißner, Phys. Lett. B **500**, 263 (2001).
- [37] A.D. Martin, Nucl. Phys. **B179**, 33 (1981).
- [38] M.Th. Keil, G. Penner, and U. Mosel, Phys. Rev. C **63**, 045202 (2001).
- [39] T. Waas, N. Kaiser, and W. Weise, Phys. Lett. B **379**, 34 (1996); M. Lutz, *ibid.* **426**, 12 (1998).
- [40] A. Ramos and E. Oset, Nucl. Phys. **A671**, 481 (2000).
- [41] J. Schaffner-Bielich, V. Koch, and M. Effenberger, Nucl. Phys. **A669**, 153 (2000).
- [42] L. Tolós, A. Ramos, A. Polls, and T.T.S. Kuo, Nucl. Phys. **A690**, 547 (2001); L. Tolós, A. Ramos, and A. Polls, Phys. Rev. C **65**, 054907 (2002).
- [43] M.F.M. Lutz and C.L. Korpa, Nucl. Phys. **A700**, 309 (2002).
- [44] G. Höhler, in *Numerical Data and Functional Relationships in Science and Technology*, edited by H. Schopper, Landolt-

- Börstein, New Series, Group I, Vol. 9B, part 2 (Springer, Berlin, 1983).
- [45] B. Holzenkamp, K. Holinde, and J. Speth, Nucl. Phys. **A500**, 485 (1989).
- [46] T. O. Ericson and W. Weise, *Pions in Nuclei* (Clarendon, Oxford, 1988).
- [47] L.L. Foldy and J.D. Walecka, Ann. Phys. (N.Y.) **36**, 447 (1969); V.R. Pandharipande and H.A. Bethe, Phys. Rev. C **7**, 1312 (1973).
- [48] M.B. Johnson, H.A. Bethe, Nucl. Phys. **A305**, 418 (1978); M.B. Johnson and B.D. Keister, *ibid.* **A305**, 461 (1978).
- [49] G.E. Brown, S.O. Bäckman, E. Oset, and W. Weise, Nucl. Phys. **A286**, 191 (1977); E. Oset, H. Toki, and W. Weise, Phys. Rep. **83**, 281 (1982).
- [50] A. L. Fetter and J. D. Walecka, *Quantum Theory of Many-Particle Systems* (McGraw-Hill, New York, 1971).
- [51] M. Ericson and T.E.O. Ericson, Ann. Phys. (N.Y.) **36**, 323 (1966).
- [52] G. Fäldt, Nucl. Phys. **A206**, 176 (1973).
- [53] V.R. Pandharipande, C.J. Pethick, and V. Thorsson, Phys. Rev. Lett. **75**, 4567 (1995).
- [54] T. Waas, M. Rho, and W. Weise, Nucl. Phys. **A617**, 449 (1997).
- [55] W. Weise, Nucl. Phys. **A278**, 402 (1977).
- [56] A. B. Migdal, *Theory of Finite Fermi Systems and Application to Atomic Nuclei* (Wiley, New York, 1967).
- [57] G. Baym and G.E. Brown, Nucl. Phys. **A247**, 395 (1975).
- [58] H. Heiselberg, C.J. Pethick, and E.F. Staubo, Phys. Rev. Lett. **70**, 1355 (1993).
- [59] D.N. Voskresensky, M. Yasuhira, and T. Tatsumi, Phys. Lett. B **541**, 93 (2002); nucl-th/0208067.
- [60] N.K. Glendenning, Phys. Rev. D **46**, 1274 (1992).
- [61] M. Christiansen, N.K. Glendenning, and J. Schaffner-Bielich, Phys. Rev. C **62**, 025804 (2000).
- [62] N. Glendenning, Phys. Rep. **342**, 393 (2001).
- [63] H. Heiselberg and M. Hjorth-Jensen, astro-ph/9904214.
- [64] Yu.B. Ivanov, J. Knoll, and D.N. Voskresensky, Nucl. Phys. **A672**, 313 (2000).
- [65] J. Knoll and D.N. Voskresensky, Ann. Phys. (N.Y.) **249**, 532 (1996).
- [66] A.B. Migdal, Rev. Mod. Phys. **50**, 107 (1978).
- [67] A.M. Dyugaev, Zh. EksP. Teor. Fiz. **83**, 1005 (1982) [Sov. J. Nucl. Phys. **38**, 680 (1983)].
- [68] D.N. Voskresensky and I.N. Mishustin, JETP Lett. **34**, 303 (1981); Sov. J. Nucl. Phys. **35**, 667 (1982).
- [69] D.N. Voskresensky, Phys. Lett. B **358**, 1 (1995).
- [70] D.N. Voskresensky, Lect. Notes Phys. **578**, 467 (2001); astro-ph/0101514.
- [71] E. E Saperstein and S.V. Tolokonnikov, JETP Lett. **68**, 553 (1998); S.A. Fayans and D. Zawischa, Phys. Lett. B **363**, 12 (1995); I.N. Borzov, S.V. Tolokonnikov, and S.A. Fayans, Sov. J. Nucl. Phys. **40**, 732 (1984).